KLIMA 2050

A MONITORED UNSATURATED SLOPE IN NORWAY: EIDSVOLL CASE STUDY

Luca Piciullo, Vittoria Capobianco and Håkon Heyerdahl

KLIMA
2050

Preface

The main aim for this pilot project is to transform the real-time monitoring into an early warning system useful to issue warnings for the road and railway authority. Currently the work is focused on defining a reliable hydrological model able to back calculate the hydrogeological variables measured in the slope. Further analyses will be focused on the definition of triggering thresholds to be employed in the early warning system. A slope stability software and machine learning algorithms will be employed to determine the triggering values as a function of the main input (rainfall, snowmelt, temperature, vegetation). The approach being developed for this pilot will be available for adaptation and implementation as a slope scale Landslide Early Warning System (LEWS) to forecast the occurrence of landslides and prevent fatalities and damages.

Klima 2050 - Risk reduction through climate adaptation of buildings and infrastructure is a Centre for Research-based Innovation (SFI) financed by the Research Council of Norway and the consortium partners. The SFI status enables long-term research in close collaboration with private and public sector, as well as other research partners aiming to strengthen Norway's innovation ability and competitiveness within climate adaptation. The composition of the consortium is vital in order to being able to reduce the societal risks associated with climate change.

The Centre will strengthen companies' innovation capacity through a focus on long-term research. It is also a clear objective to facilitate close cooperation between R&D-performing companies and prominent research groups. Emphasis will be placed on development of moisture-resilient buildings, stormwater management, blue-green solutions, measures for prevention of water-triggered landslides, socio-economic incentives and decision-making processes. Both extreme weather and gradual changes in the climate will be addressed.

The host institution for SFI Klima 2050 is SINTEF, and the Centre is directed in cooperation with NTNU. The other research partners are BI Norwegian Business School, Norwegian Geotechnical Institute (NGI), and Norwegian Meteorological Institute (MET).

The business partners represent important parts of Norwegian building industry; consultants, entrepreneurs and producers of construction materials and technology: Skanska Norway, Multiconsult AS, Mesterhus, Norgeshus AS, Leca AS, Isola AS and Skjæveland Gruppen AS. The Centre also includes important public builders and property developers: Statsbygg, Statens vegvesen, Jernbanedirektoratet and Avinor AS. Key actors are also Trondheim kommune, The Norwegian Water Resources and Energy Directorate (NVE) and Finance Norway.

Trondheim, June 2022

Berit Time
Centre Director/Senterleder
SINTEF Community

Summary

In steep unsaturated slopes, the unsaturated region has a crucial role in maintaining the slope stability. In this work, the hydrological behaviour of a natural unsaturated slope located adjacent to a railway track in Eastern Norway has been modelled. Due to its steep inclination, the slope is monitored, and its stability is kept under frequent observation. The commercial software GeoStudio was used to create and calibrate a model able to replicate the in-situ monitored soil water content conditions. Six simulations were carried out by changing the initial and boundary climate conditions of the slope. The simulations conducted were divided into two main series: one with an initial calibration of the VWC profile (C), and another with no calibration (NC). For each of them, three different surface boundary conditions were applied: i) only precipitation, ii) precipitation and atmospheric conditions, iii) precipitation, atmospheric conditions and vegetation, according to the Penman-Monteith equation for evapotranspiration. The simulations have been validated though the use of Taylor diagrams that graphically summarize how closely a pattern (or a set of patterns) matches observations. The results show that including an initial calibration, climate conditions and vegetation, is crucial to best model the response of an unsaturated slope in Norway. The effectiveness of the best simulation in back-calculating soil water content, was tested for 3 different time periods: 3-month, 6-month, 1-year. The results show that the hydrological model can adequately represent the real monitored conditions up to a 6-month period, afterward a recalibration is needed. In addition, a coupled seepage and slope stability analysis for the 6-month period has been carried out. The calculated FS varies up to 18% depending on the complexity of the boundary conditions used in the model. The findings of this work can be seen as a preliminary step towards a real-time slope stability analysis and local landslide early warning system (Lo-LEWS).

Content

1   Introduction

Future climate in the Nordic region is forecasted to be warmer, wetter, and more erratic with respect to freeze-thaw and wetting-drying cycles (Hanssen-Bauer et al. 2017). Intelligent solutions to hazard and risk management must be developed to safeguard society and infrastructure to climate-induced geohazards. Prone-to-failure slopes, especially if located in vulnerable areas, need proper monitoring as the rainfall patterns change quickly, and predisposing factors leading to slope instability must be tracked. Water infiltration into soil is one of the main triggering factors of slope instability, since it results in an increase of volumetric water content and simultaneously a reduction of matric suction and thus shear strength, which may trigger slope failure (Anderson and Sitar 1995; Alonso et al. 1995; Li et al. 2005; Lu et al. 2010). The infiltration into the soil is mostly affected by the soil hydraulic characteristics and the permeability of the soil-bedrock interface, if present (Greco et al. 2017).   In Nordic regions, another important factor that affects the water infiltration is the snowmelt, which usually cannot be neglected.

The evaporation of water from the ground surface is another important factor that generally increases soil suction due to an outwards water flux. However, evaporation is often neglected or rarely considered and, in slope stability problems, both rainfall infiltration and evaporation are included in extremely simplified ways through an entering or exiting water flow. Furthermore, experimental studies conducted on the hydraulic response of pyroclastic ashy soils on evapotranspiration and rainfall infiltration (Rianna et al. 2014; Pagano et al. 2014; Fusco et al. 2019) outlined that neglecting vegetation can lead to incorrect estimation of the pore-water pressure regime over long time periods.

In fact, some authors started to evaluate hydrological responses of these soils by considering also the presence of vegetation (Comegna et al., 2013; Pagano et al., 2019; Capobianco et al., 2020), which may play an important role in stabilizing unsaturated slopes. Densely vegetated slopes appear to be less prone to shallow landslides also due to the apparent cohesion that the root system provide to the shallowest layers, the interception provided by the aboveground vegetation, and the potential bedrock weathering (when present) due to the presence of the roots (McGuire et al. 2016).

Many authors have studied the response to rainfall of partially saturated soils in natural slopes. Examples can be found for volcanic soils in Italy (Casagli et al. 2006; Cascini et al. 2010; De Vita et al. 2013), residual soils in Hong Kong and Singapore (Ng and Pang 2000; Li et al. 2005; Rahardjo et al. 2005; Rahimi et al. 2011), silty sand and silty clay in India (Sarma et al. 2015), flysch materials in Croatia (Peranic et al., 2019), and in bluffs in Washington area, USA (Godt et al. 2008). Few studies on partially saturated soils along streambanks in Norway focused on the climate and vegetation-driven hydraulic changes of the slope and how these would affect the stability of the slope (Krzeminska et al., 2019; Capobianco et al., 2021), but studies on natural slopes are still lacking, and it is becoming of crucial importance to document how these respond to the increased amount of intense rainfall and rapid snowmelt.

This study proposes a four-phase approach to set up a near-real-time stability analysis and warning system at slope scale (Piciullo et al., 2018). Before being able to conduct a complete near-real-time stability analysis, a proper assessment of the behaviour of the unsaturated soils is essential. Recently, Li et al (2020) proposed a Web-GIS-based model for the analytical assessment of the near-real-time stability evaluation of regional soil slopes under complex rainfall conditions. However, the model was not able to fit well the numerical modelling when the inclination of the slope was higher than 25°.

The methodology proposed in this study is applied to a monitored steep slope in Norway, with a focus on the first two phases of the proposed approach (monitoring and modelling). The slope under investigation has been monitored since 2016 and has been included as a pilot study within the Center for Research-based Innovation (CRI) Klima2050 (http://www.klima2050.no/). The most reliable hydrological model has been defined validating the results of 6 different simulations with in-situ measurements using Taylor diagrams. In addition, the effectiveness of the hydrological model was tested for different time spans: 3-month, 6-month, 1 year. The results highlighted the importance of including rainfall, snowmelt, climate variables and vegetation cover, for a better estimate of the monitored variables and a more reliable slope stability evaluation.

2 Conceptualization of the near-real-time stability analysis and warning at slope scale

Rainfall-induced landslide are usually triggered by a combination of wet antecedent conditions followed by one or more days of relatively intense rainfall (Baum et al. 2005). The transient reduction of suction during infiltration and, thus, increment of soil water content, can be used to identify periods when stress and moisture conditions concurring to sliding with rainfall in unsaturated slopes (Godt et al. 2009). Identifying the conditions that may lead to the potential failure of a slope, can help defining threshold values for landslide early warning purposes. Figure 1 proposes a workflow including the main parts of a near-real-time slope stability analysis, based on hydrological monitoring of a landslide at a slope scale (Piciullo et al., 2018). The approach implies four main phases: monitoring, modelling, forecasting and warning. The monitoring phase is necessary to provide the input data to the modelling phase. The monitored data, specifically hydrological (i.e. pore water pressure regime, soil water content) and climate data (i.e. daily and hourly rainfall, snowmelt, air temperature, relative humidity, wind speed) are used as input parameters for the hydrological modelling together with the soil properties. These latter are usually obtained by laboratory or field tests.

The calibration of the model consists in fine-tuning the initial hydraulic conditions to fit as much as possible the measured data. The climate data are inputted as water flux boundary conditions. The water flux can be either extremely simplified, i.e. an entering water flux simulating the rainfall infiltration, or it can include additional factors, such as plant evapotranspiration, interception, and runoff. When evapotranspiration is included, additional climate variables are needed to the model to solve the Penman-Monteith equation (Allen et al., 1998), together with vegetation properties, as discussed more in detail in Section 5. During the calibration phase, daily atmospheric data can reasonably be used as input to the model. The validation consists in comparing predicted (by the model) and observed (by in-situ monitoring) hydrological data to define the best simulation fitting the real conditions, for a certain time span.

The best simulation obtained with the hydrological modelling is then used for the slope stability modelling. Finally, the results of the slope stability modelling are used to identify combinations of hydrological variables and precipitation that may lead to the slope failure (i.e., Factor of Safety (FS) less than 1). At this stage, the monitored variables, precipitation and the results of the slope stability modelling can be the inputs for training machine learning algorithms to detect combinations of variables that lead to FS<1. In the forecast phase, predicted values of precipitation can be used as input data for machine learning algorithms, with the aim of predicting time frames where slope instabilities are likely to occur. When thresholds are exceeded or FS values less than 1 are detected, warning protocols and emergency plans need to be activated.
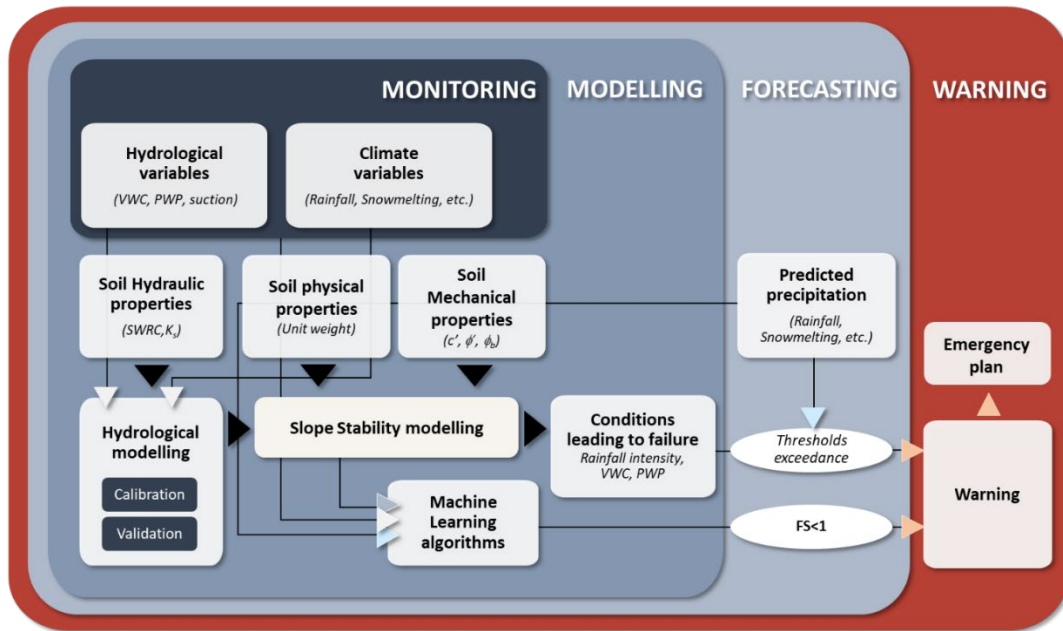
Figure 1. Conceptualization of the phases for a near real-time slope stability analysis and warning at a slope scale.

3   The case study

3.1   Study area and monitoring system

The study area is located in the municipality of Eidsvoll, Norway (60° 19' 23.376", 11° 14' 44.646", Figure 2). The slope under analysis is 25-30 m high, with an inclination of about 45° in the upper part. As part of an InterCity railway project in Eastern Norway, an additional railway track is being constructed next to an existing railway line at its toe. The slope has not shown any deformations so far, but it represents a threat to both the existing railway line and the proposed new one. In addition, the slope is located at the eastern side of a cultural heritage area, with an old church from the 12th century and its graveyard, which makes impossible the realization of physical slope stability measures. For the above-described reasons, the slope is instrumented with several sensors.
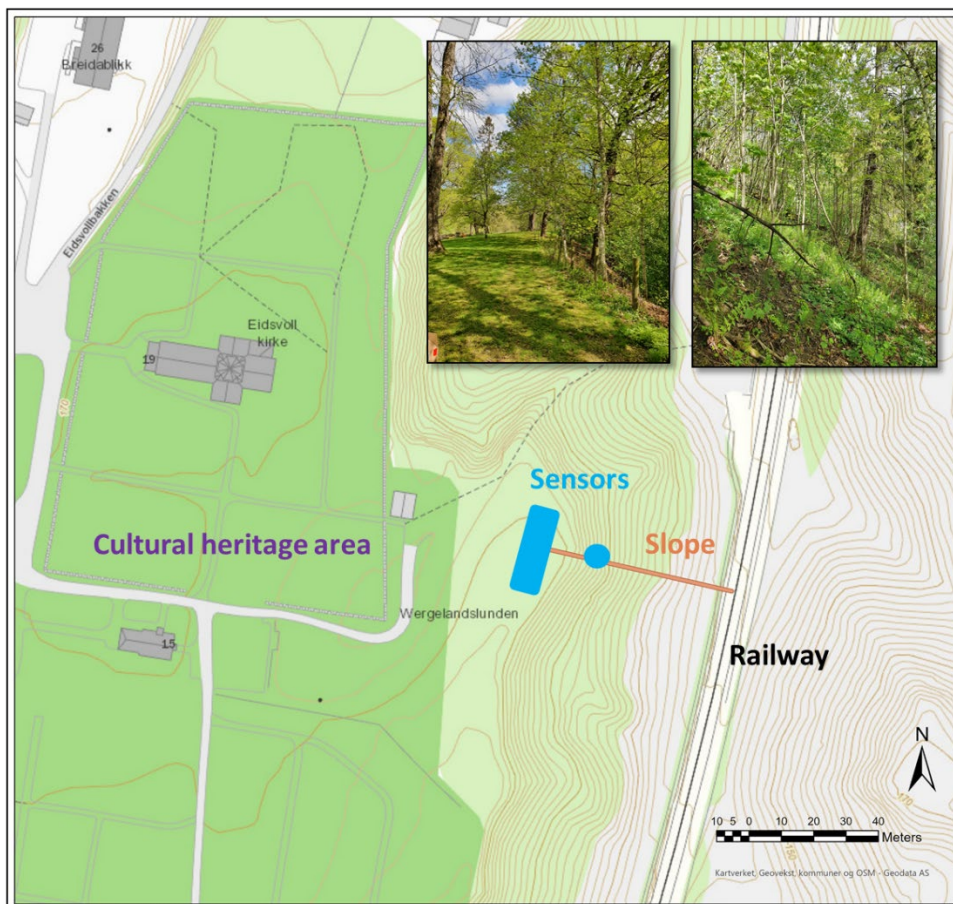
Figure 2 The pilot site at Eidsvoll, central south Norway. Slope, sensors and railway location. Eidsvoll church (kirke) and the cemetery surrounding it are protected.

Volumetric water content (VWC) and pore-water pressure (PWP) sensors were installed in late spring/early summer of 2016 (Heyerdahl et al, 2018) to monitor the hydrological conditions. The VWC sensors use an electromagnetic field to measure the dielectric permittivity of the surrounding medium. Electric piezometers are used to measure the pore water pressure.

Grain size distribution analyses have been carried out for several representative samples taken at different depths (Heyerdahl et al, 2018). The results have been interpreted identifying the following three layers, from the top: a sand/silt layer of circa 6 meters, a

smaller layer of clayey silt material (about 3 meters thick), a firm marine clay layer to large depths (Figure 3).

In the top layer of the sand/silt, sensors are installed for the combined measurement of VWC and ground temperature. The installation depths are respectively at 0.1 m, 0.5 m, 1 m, 2 m, 4 m and 6 m. In addition, electric piezometers have been installed respectively at 6 m, 9 m, 15 m and 23 m depth. The two deepest piezometers (15 m and 23 m) are located within the clay layer (layer 3 in Figure 3). The piezometer sensor at 9 m depth is in a transition zone between silt and clay layers, while the uppermost piezometer (6 m) is installed in the silt layer. Figure 3 shows the position of sensors in a slope cross section. The VWC and PWP sensors are monitored in real-time with 1-hour frequency. Readings are collected online through Deltalink-cloud software (https://deltalink-cloud.com/#/auth/login).
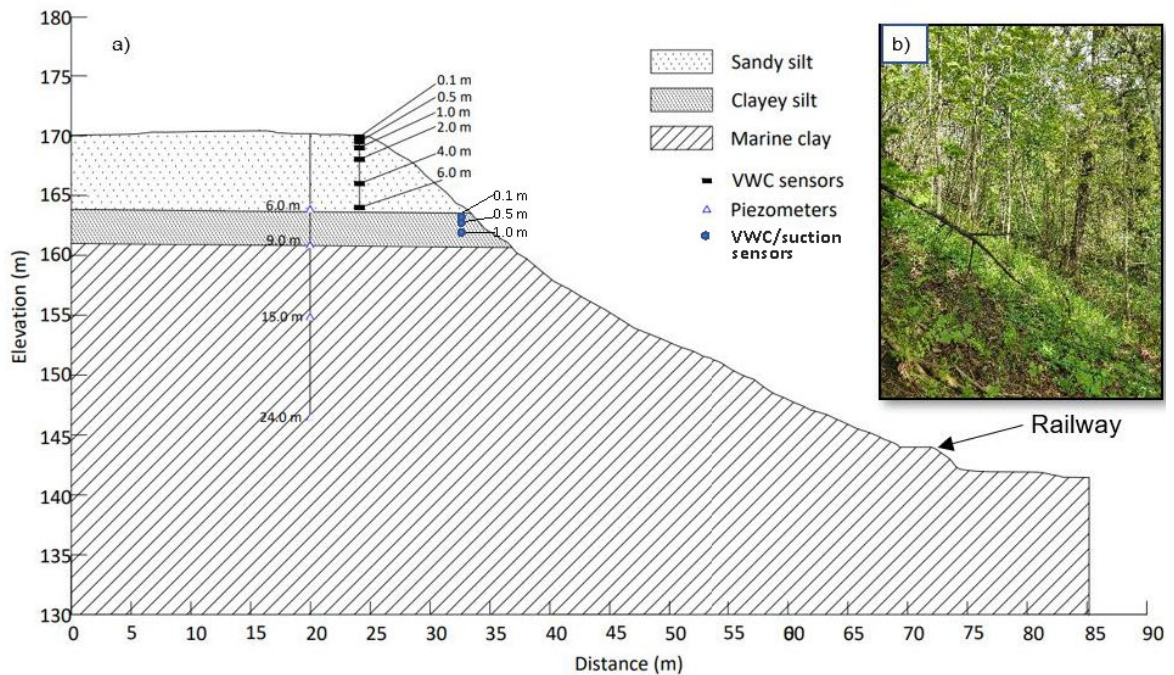
Figure 3 Schematic cross section of the studied slope (Figure 2) and depth location of the sensors.

The area is exposed to frequent and long-term rainfall events, especially in the fall. In the autumn 2000, many landslides were triggered by extreme long-term rainfall that occurred in the Eastern part of Norway. The highest measured rainfall in that year corresponded to a return period of approximately 100 years. No deformations were recorded at the slope location, but as landslides are likely to become more frequent with climate change (Gariano and Guzzetti 2016), the need of a real-time monitoring for situational awareness of slope stability is becoming urgent.

3.2 New sensors installed

On the 27th of May 2021, two sensor types have been installed on the slope of pilot case study in Eidsvoll for measuring volumetric water content and soil suction. Specifically, TEROS 12 determines VWC using capacitance/frequency-domain technology. The sensor uses a 70-MHz frequency, which minimizes textural and salinity effects. TEROS 12 sensor measures volumetric water content between Needle 1 and Needle 2 and electrical conductivity between Needle 2 and Needle 3 (Figure 4a). Temperature is measured with an embedded thermistor. More info can be found on TEROS11-12_Manual.

The TEROS 21 sensor measures the suction and temperature of soil with porous ceramic discs (Figure 4b). The ceramic used with the TEROS 21 has a wide pore size distribution and is consistent between discs, giving each disc the same moisture characteristic curve. Thus, the water potential can be inferred from water content using the moisture characteristic curve of the ceramic. As the sensor dries past the plant-available range, the total pore volume that drains at a given water potential decreases. At these low water potentials, the measured water potential can become somewhat noisy because small changes in measured water content of the ceramic translate into large changes in water potential. This phenomenon is most pronounced when the sensor is air dry. It is expected that the measured water potential of a dry sensor open to the air can jump around significantly. The noise level is much lower when the sensor is installed in the soil, even at air-dry water potential.

The air entry potential of the largest pores in the ceramic is about −9 kPa. However, the ceramic disc must have access to air for the large pores to begin draining and the response of the sensor to change. If the soil around the sensor has an air entry potential lower (drier) than −9 kPa, the ceramic will not begin to lose water until reaching the air entry potential of the soil. In this scenario, the air entry potential of the soil limits the wet-end range, rather than the ceramic discs themselves. The sensor may not begin to respond until lower water potentials. This is generally only an issue when using the sensor in poorly structured soils with high clay content. METER performs TEROS 21 calibration on the drying leg of the hysteresis loop, so the measurements are most accurate as the soil dries. Measurements as the soil wets up are slightly drier (more negative water potential) than the true water potential of the soil. METER wetting and drying tests show the magnitude of the hysteresis error is <10 kPa in the −20 to −100 kPa range.

The water potential range for TEROS 21 is plotted in Figure 5.
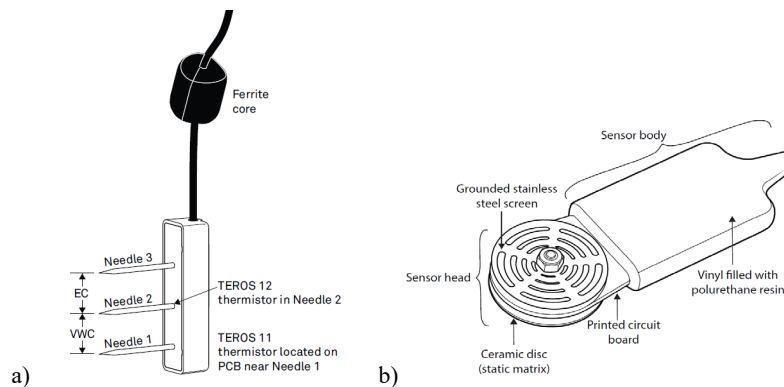
Figure 4: a) TEROS 12 sensor for volumetric water content measurements; b) TEROS 21 sensor for soil suction measurements.
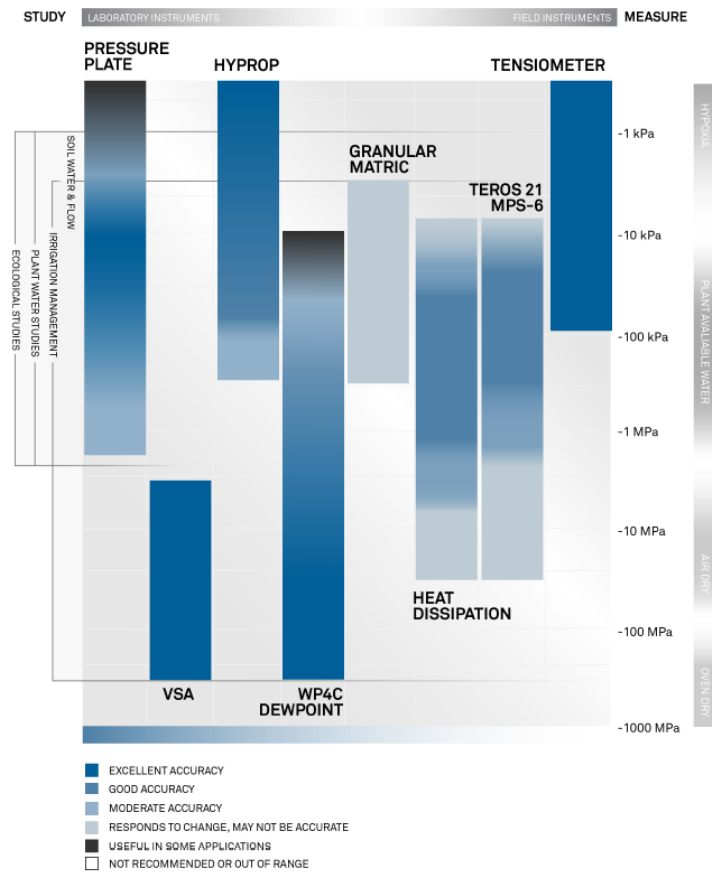
Figure 5: Water potential instrument ranges (TEROS21_Manual).

A total number of six sensors, three of the TEROS12 type and three of the TEROS21 type, have been installed. The installation has been carried out at three different depths, 0.1m (Figure 6a), 0.5m and 0.9 m, coupling the two sensor types. All the sensors are connected to a datalogger (ZL6). The ZL6 has an integrated solar panel to recharge NiMH batteries.

Figure 6: a) installation of sensors at depth of 0.1m; b) Datalogger.

The ZL6 transmits data to ZENTRA Cloud servers, and it is possible to visualize them on line (Figure 7). The data can be recorded with a 5-minute interval and the data transmitted every hour. To save battery, the data are currently recorded every hour and transmitted to the cloud every morning. All the sensors and the datalogger belong to the METER group.

Figure 7: Data available on Zentra cloud web platform.

3.3 Monitoring data

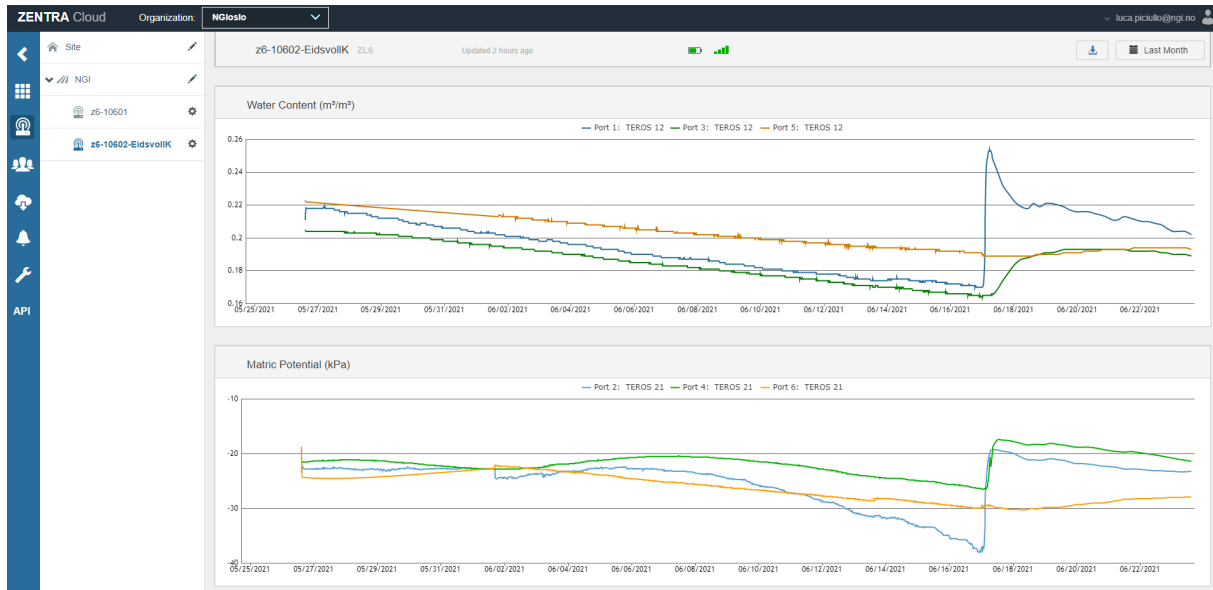Monitoring of the PWP and VWC started in May 2016 (Figure 8). The soil temperature is also monitored at each depth (Figure 8c). The measurements were processed to remove unreliable values (i.e. VWC < 0%), due to either maintenance or contact problems (Figure 8a, c). Although there is a lack of data for PWP between February 2017 and March 2019 (Figure 8a), it is possible to observe that the PWP values at 9 m, 15 m and 23 m, remained almost constant, after the first month of stabilization due to the installation. The PWP measured by the 4 piezometers indicates that the water table is at 7 meters depth from the surface, with negative values of about -10 kPa measured at 6 m. From October 2019, a PWP increase is observed, until a peak of about 6 kPa is reached around April, after which the PWP decrease again with the beginning of the summer season. This fluctuation of the PWP– from 10 kPa to 6 kPa indicate that the water table changes seasonally from 7 meters depth in spring-summer to 5.5-6 meters in fall-winter.

The VWC is influenced by both freezing and snow melting periods. Freezing periods can be easily detected by the soil temperature reaching values below 0°C, while snow melting is typical occurring in spring. Temperature and precipitation values are shown in Figure 8c, where precipitation accounts for both daily rainfall and daily snowmelt. Drops in logged VWC due to pore water transformed into ice were observed at shallow depths (0.1 m and 0.5 m) each year at the beginning of the winter, with the exception of the winter 2019-2020, which was exceptionally warm (Figure 8c). This behaviour was confirmed by the values of temperature recorded below 0°C at the shallowest layer starting from around November 2016, 2017, 2018, except for winter 2019. It is worth mentioning that the low VWC values recorded in periods with temperature below zero do not realistically represent the in-situ soil VWC. At the beginning of the spring, with exception of 2019-2020, peaks of VWC due to snowmelt were recorded at shallow depths (Figure 8b). Smaller peaks can be observed also at 1 m depth, where the water infiltration, due to snowmelt, arrives with a delay, providing a small shift of the VWC trend. VWC values at larger depths did not show significant changes, but rather a constant behaviour, except at 6 m depth, where an initial drop was recorded, which then stabilized throughout the years.

The meteorological variables used for modelling, such as rainfall, snowmelt, air temperature, relative humidity and wind speed were taken from the Norwegian website senorge.no (http://www.senorge.no). The precipitation (rainfall and snowmelt) dataset is a daily gridded raster file evaluated combining weather station and radar measurements. Snowmelt was estimated by the Snow map model (Lawrence et al., 2009; Saloranta, 2012).
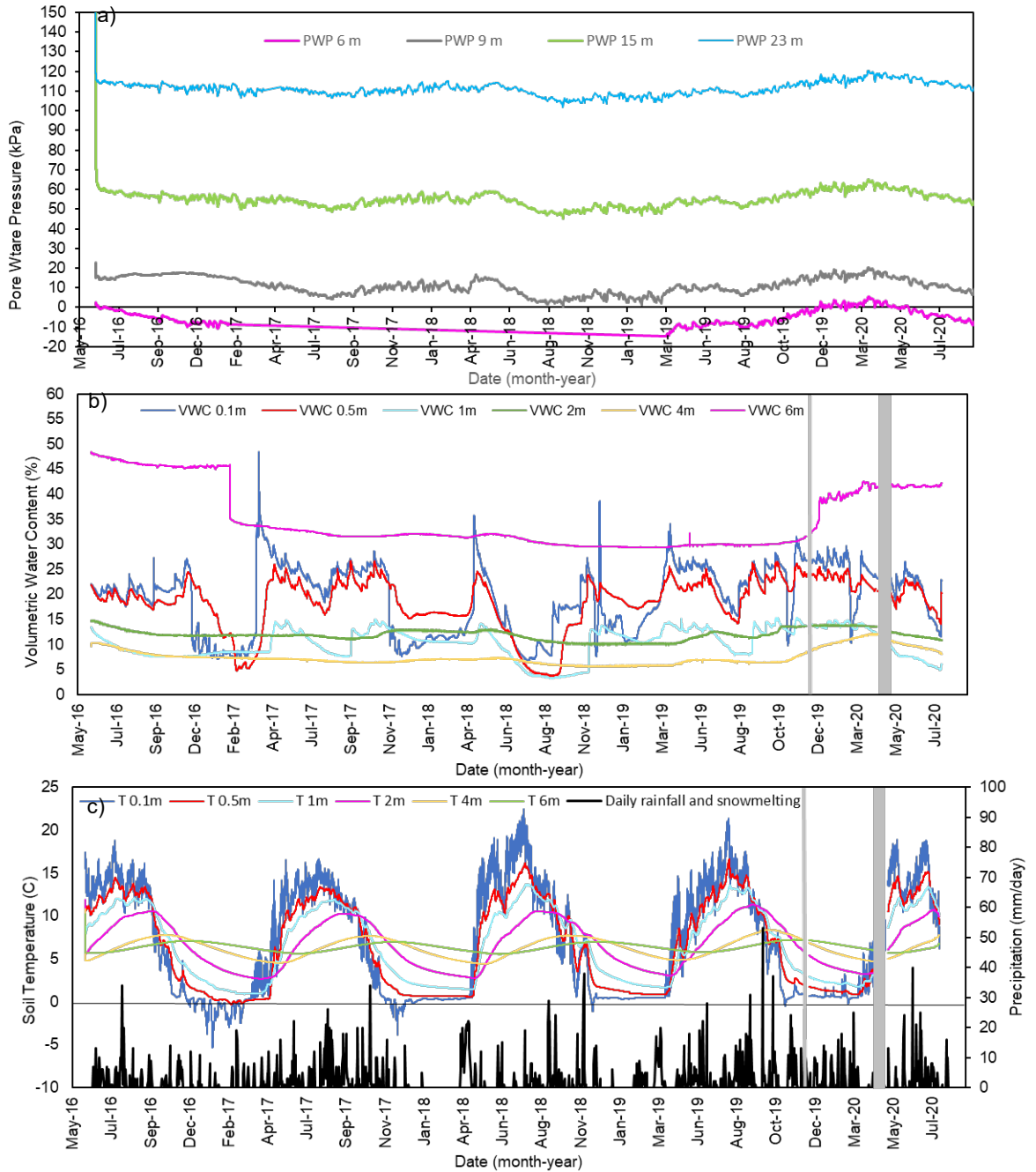
Figure 8. a) Pore-water pressures monitored at four depths of the instrumented slope from May 2016 to August 2020; b) VWC monitoring data at six depths of the instrumented slope from May 2016 until August 2020 (the grey bars represent the periods with data unavailability, due to either maintenance or contact problems.); c) Monitored temperature at six depths of the instrumented slope and rainfall-snowmelt data from senorge.no.

4   Numerical modelling

4.1   GeoStudio – SEEP module

The commercial software GeoStudio (GEO-SLOPE International, Ltd.) was used to perform the numerical analyses. Two modules of the software were combined, namely SEEP/W (analysis of unsaturated groundwater flow) and SLOPE/W (slope stability computation), to determine the influence of climate drivers (air temperature, relative humidity, solar radiation etc.), vegetation, rainfall and snowmelt infiltration on the slope stability. The 2D finite element module SEEP/W was used to analyse the transient seepage and obtain the pore-water pressure distribution and soil VWC variation with time in the soil. The governing equation in SEEP/W is Richards' equation (Richards, 1931 and Childs and Collis-George, 1950), which describes two-dimensional flow in unsaturated soils, as shown in eq (1)

$$\partial/\partial x \, (k_x \, \partial h/\partial x) + \partial/\partial y \, (k_y \, \partial h/\partial y) + Q = \partial\theta/\partial t \qquad (1)$$

where x and y are spatial coordinates; θ is the volumetric water content; h is the hydraulic head; kx and ky are a function of θ and represent the hydraulic conductivities in the x and y directions, respectively; Q is water flux; and t is time.

The SEEP/W transient analyses, saved every 24h, were used as input in the form of a pore-water pressure distribution for the slope stability analysis. The SLOPE/W module was used to perform slope stability analysis using the limit equilibrium method (LEM) and calculation of the safety factor assuming the rotational failure model proposed by Morgenstern-Price (1965). The slope stability modelling was conducted considering the results of the SEEP/W analysis as input with a 24h step interval (see Section 4.1). Examples of numerical modelling coupling transient seepage and slope stability analyses are available in literature, to assess rainfall infiltration effects on riverbank stability (Duong et al., 2019; Capobianco et al., 2021) and on a residual soil (Heyerdahl et al., 2018; Peranić et al., 2019).

4.2   Calibration and validation procedures of the volumetric water content (VWC)

The analyses with SEEP/W were carried out starting from June 2019. At the beginning of the selected period of analysis the VWC in the soil was influenced by antecedent precipitation conditions and evapotranspiration processes. With the SEEP/W software it is not possible to manually assign a customized VWC profile before starting the simulation. To overcome this issue, the calibration procedure consisted in fitting the VWC profile measured in the soil, with the modelled one, acting on the input water flux (see Section 5.3). The calibration procedure was performed before starting the simulations. A comparison of the back-analysed results obtained with and without calibration is provided in Section 5.

For validation purposes, the results of SEEP/W simulations were compared to the observed data. The agreement between in-situ measured, i.e., observed, and modelled, i.e., predicted, VWC was evaluated considering an approach used for satellite-based soil moisture products (Albergel et al., 2012; Liu et al., 2018) and global climate models. Taylor diagrams (Taylor, 2001) were used to describe the statistical relationship between predicted and observed data. The correlation coefficient (R, eq. 2), the normalised standard deviation (SDV, eq. 3) and the centred root-mean-square difference (RMSD, eq. 4) were used to quantify the agreement between the variable predicted by different simulations and the one measured. Moreover, the bias was also calculated and included in the diagram (eq. 5). Taylor diagrams were finally

used to plot the results from the different comparison simulations-observation in a single graph per each monitored depth.

$$R = \frac{\sum_{i=1}^{n}\left[(VSWC_{pre,i} - \overline{VWC_{pre}}) * (VSWC_{obs,i} - \overline{VWC_{obs}})\right]}{\sqrt{\sum_{i=1}^{n}(VSWC_{obs,i} - \overline{VWC_{obs}})^2} * \sqrt{\sum_{i=1}^{n}(VSWC_{pre,i} - \overline{VWC_{pre}})^2}} \tag{2}$$

$$SDV = \frac{\sigma_{pre}}{\sigma_{obs}} \tag{3}$$

$$RMSD = \sqrt{\frac{\sum_{i=1}^{n}\left[(VSWC_{pre,i} - \overline{VWC_{pre}}) - (VSWC_{obs,i} - \overline{VWC_{obs}})\right]^2}{n}} \tag{4}$$

$$\text{Bias} = \frac{\sum_{i=1}^{n}\left[VSWC_{pre,i} - VSWC_{obs,i}\right]}{n} \tag{5}$$

The R, SDV, centred RMSD are related by the following normalized formula:

$$centred\ RMSD^2 = SDV^2 + 1 - 2 * SDV * R \tag{6}$$

The construction of the diagram is based on the similarity of the above equation and the Law of Cosines (Taylor, 2001):

$$c^2 = a^2 + b^2 - 2 * a * b * cos\theta \tag{7}$$

5   Inputs and analysis settings

5.1   Soil properties

According to field investigations conducted in the area and laboratory tests performed, such as pressure plate test, triaxial tests (Heyerdahl et al, 2018), the layering of the slope consists, from the top, of a 6-meter unsaturated sandy silt, followed by a 3-meter layer of clayey silt, in partially saturated condition, laying on top of a firm marine clay extending to large depth (Table 1). Natural gravimetric water content values were measured on samples taken at different depths. More than 1 sample was taken from each layer, thus, in Table 1, the range of water content is indicated for each soil type.

Table 1- Slope layers and conditions.

Layer	Soil type	Elevation (m)	Layer thickness (m)	Range of natural gravimetric water content (%)	Saturated water content (measured in lab) (%)	Conditions
1	Sandy silt	164-170	6	12-20	45	Unsaturated
2	Clayey silt	161-164	3	24-29	45	Unsaturated/ saturated
3	Firm marine clay	130-161	> 30	>29%	-	Saturated

Material properties were obtained: by triaxial tests (Heyerdahl et al, 2018) for the sandy silt layer; by literature (Statens Vegvesen, 2018; Melchiorre and Frattini, 2012) for the clayey silt and clay layers. The values are summarized in Table 2. The friction angle values are described and commented in a former study (Heyerdahl et al., 2018). To be conservative, the unsaturated shear strength angle (ϕ^b), representing shear strength increase due to the matric suction (Fredlund and Rahardjo, 1993), was considered equal to $\phi'/2$, and no additional unsaturated strength was considered as function of the VWC (Vanapalli et al., 1996). The extended Mohr-Coulomb failure envelope (Fredlund et al., 1978) was used to define the shear strength criteria as shown in equation (7):

$$\tau = c' + (\sigma - u_a)tan\phi'' + (u_a - u_w)\,tan\phi^b \qquad (7)$$

Where τ is the shear stress on the failure plane at failure; c' the intercept of the "extended" Mohr-Coulomb failure envelope on the shear stress axis when the net normal stress and the matric suction at failure are equal to zero, also referred as the "effective cohesion"; $(\sigma - u_a)$ the net normal stress at failure; ϕ' the angle of internal friction associated with the net normal stress state variable; $(u_a - u_w)$ the matric suction at failure and ϕ^b the angle representing shear strength increase due to the matric suction.

Table 2 - Material properties for slope stability analysis in SLOPE/W.

Layer	Unit weight γ (kN/m³)	Cohesion c' (kPa)	Friction angle $\phi'= 2*\phi^b$ (°)	Failure envelope
1	18	8	36	Mohr-Coulomb
2	18	8	32	
3	20	5	26	

5.2   Soil water retention curves

Modelling the unsaturated part of the slope requires knowledge of the soil hydraulic properties, which can be determined through laboratory tests. The experimental soil water retention curves (SWRCs) of the unsaturated layers of the slope were obtained through pressure plate testing (Heyerdahl et al, 2018). The van Genuchten (1980) SWRC equation was used to calculate the water content as function of the matric suction as follows:

$$\theta = \theta_r + \frac{\theta_s - \theta_r}{\left[1 + \left(\frac{\psi}{\alpha}\right)^n\right]^m} \qquad (8)$$

where: θ is the actual soil water content (m³/m³); θ_r the residual water content (m³/m³); θ_s the saturated water content (m³/m³); ψ the matric suction (kPa); α is a scaling factor (kPa); n and $m=(1-1/n)$ are fit parameters of the model related to the shape of the curve.
The hydraulic conductivity was calculated as follows:

$$k_w = k_s \frac{\left[1 - (\alpha\psi^{(n-1)})\left(1 + (\alpha\psi^n)^{-m}\right)\right]^2}{\left(\left((1 + \alpha\psi^n)\right)^{\frac{m}{2}}\right)} \qquad (9)$$

where k_w is the actual hydraulic conductivity (m/s) and k_s is the saturated hydraulic conductivity.

Figure 9 shows the soil water retention curves for the drying phase obtained interpolating the results of the pressure plate tests. Batch1, Batch2 and Batch3 between 1.5 and 6 m could be considered to have comparatively equal retention properties, while Batch 4 at 6-7 m was different.
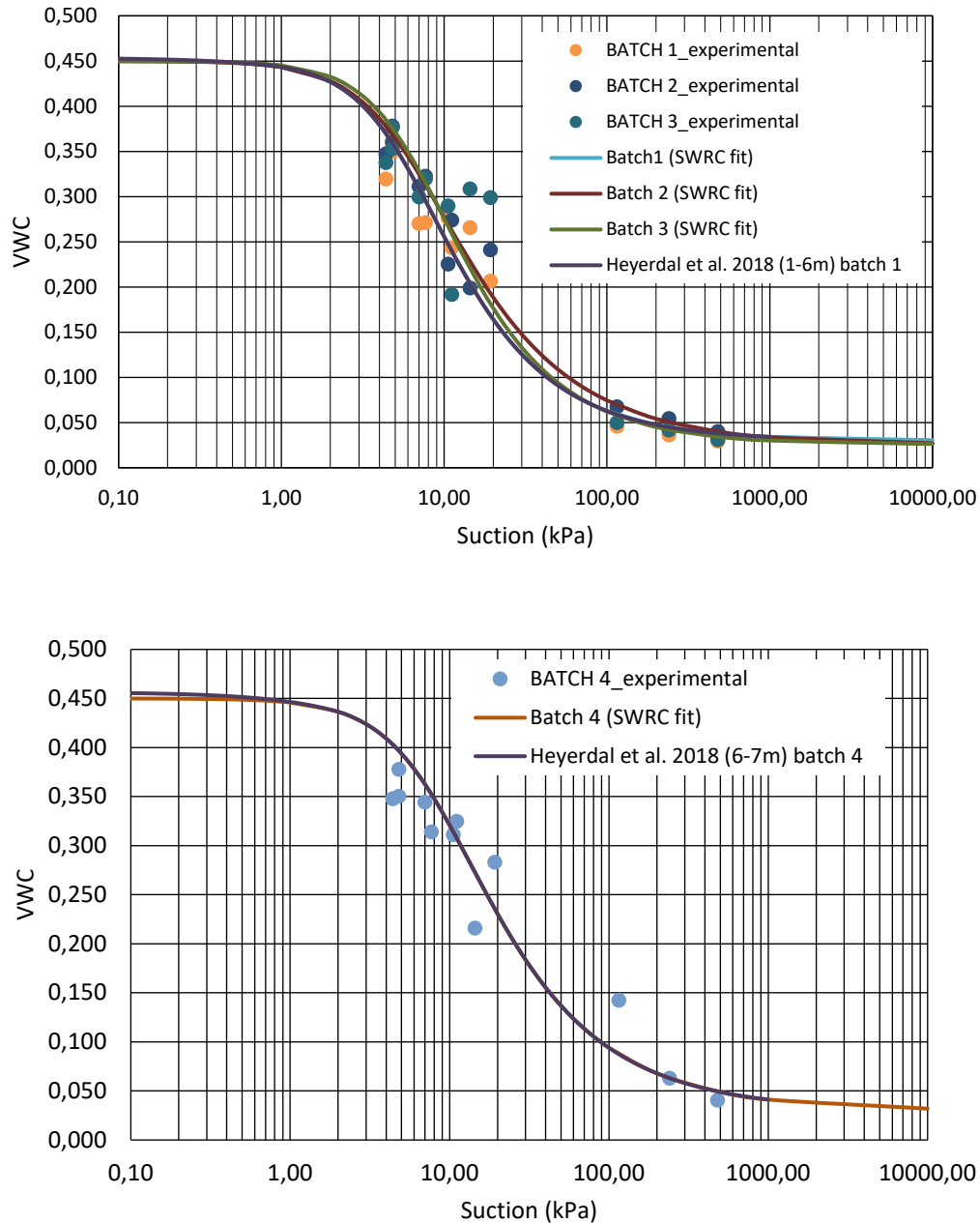
Figure 9. Soil water retention curves for the drying phase obtained interpolating the results of the pressure plate tests. a) for sand silt layer from 0 to 6-meter depth; b) for clayey silt layer from 6 to 7-meter depth.

In Table 3 the van Genuchten best-fit parameters α, n and m are shown, together with the saturated hydraulic conductivity (k_{sat}) measured with the constant head method on undisturbed specimens in the conventional triaxial apparatus (Heyerdahl et al., 2018).

It is important to specify that tests for the determination of the SWRCs during the absorption phase were not performed, thus the hysteresis in the soil retention behaviour was not taken in consideration, despite it is generally recommended to use the wetting curve, for better characterization of unsaturated flow conditions leading to slope failure (Ebel et al. 2010; Chen et al. 2017, Ebel et al. 2018).

Table 3 - van Genuchten best fit parameters for SWRC and saturated permeability. *m*=(1-1/*n*); *α*: scaling factor; θ_s: saturated water content; θ_r: residual water content; k_sat: saturated hydraulic conductivity.

Layer	n -	m -	α (kPa)	θ_s	θ_r	k_sat m/s
1	1.9	0.474	5.92	0.45	0.03	2.4E-06
2	1.76	0.432	8.47	0.45	0.03	1.0E-07

5.3   Transient seepage analyses set-up

The geometry of the slope model is shown in Figure 10. The initial ground water level (GWL) was assumed at around 7 meters depth below the surface on top of the slope, according to the PWP values recorded from the piezometers. It was assumed to follow the topographic contour on the slope at circa 1.5 meters depth. This water table profile was defined considering the 4 piezometers installed on top of the slope and 2 other piezometers at the toe of the slope located at 5 m and 12 m depth. Collected daily precipitation (rainfall and snowmelt) data were used to define the flux boundary conditions along the slope surface in the SEEP/W program. A constant head value at both the right and left boundaries were assumed, in accordance to the water level monitoring of 162 m on the left and 142 m on the right. To discretize the domain, quadrilateral and triangular elements of about 1-meter resolution were used (Figure 10), with a total of 2460 elements and 2566 nodes.
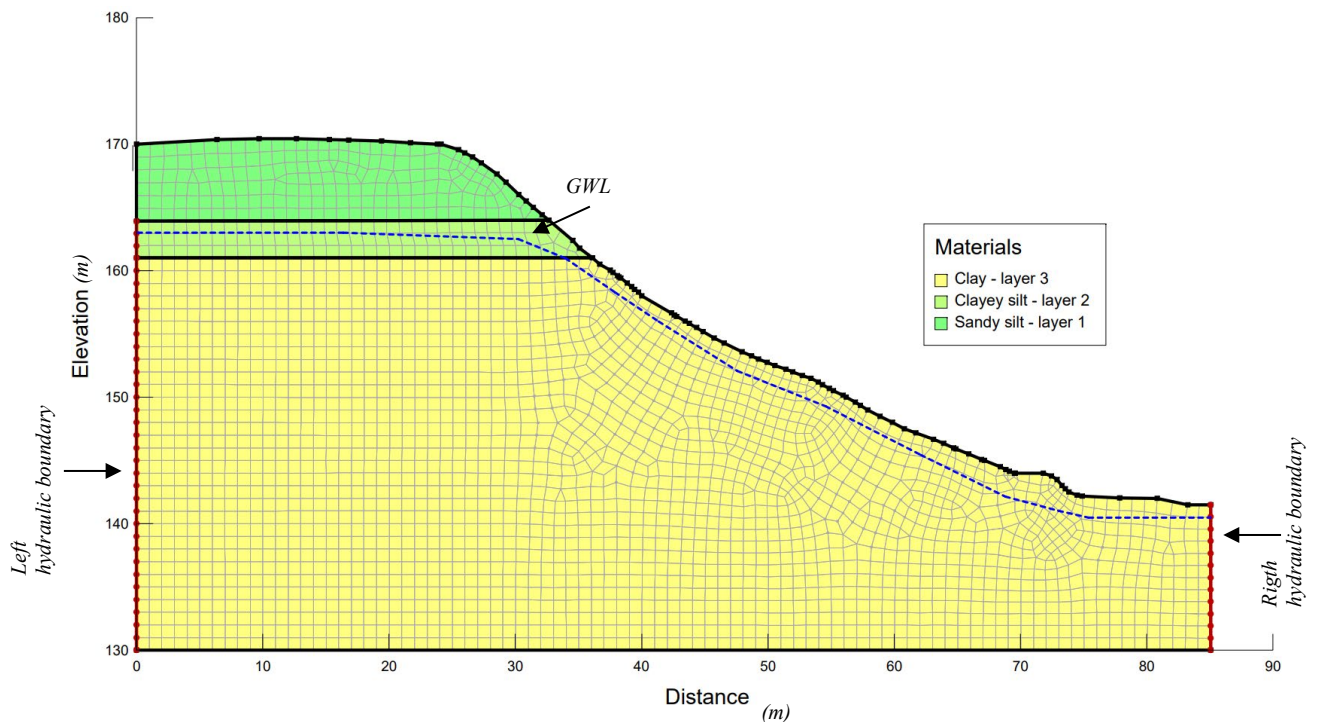
Figure 10. Slope geometry with mesh distributions and regions used in the model. The dashed blue line indicates the location of the Ground Water Level (GWL).

To assess the evaporation flux, SEEP/W module uses by default the Penman-Monteith equation (Allen et al., 1998).

To simulate the saturation conditions in the unsaturated zone in SEEP/W, the GWL is usually located first, and then the maximum negative head (MNH) can be used to build the assumption of the predetermined negative pore pressure profile. The MNH was set equal to 1.5 m, and the pore-water pressure graph was linear and negatively sloped from the

groundwater table to the MNH. However, negative pore-water pressures in a natural slope most likely do not show a linear trend. The shallowest layers are more subject to wetting cycles determined by short-term rainfall, which would slightly affect deeper layers (Comegna et al. 2016).

The measured initial VWC profile showed a non-linear trend, with an increasing VWC towards the surface from a minimum value at 4 m depth and assumed saturated conditions below 6 m depth (Figure 11). In this regard, two series of simulations starting from different initial conditions (IC) were considered: i) Non-calibrated (NC), with a linear trend of negative pressure head up to 1.5 m of MNH, and ii) Calibrated (C), with a VWC profile resulting from a preliminary hydrological adjustment (Figure 11). The calibrated VWC profile was obtained by applying an initial condition of steady-state analysis with a constant surface unit flux equal to the recorded average monthly rainfall amount of the antecedent month (180 mm).
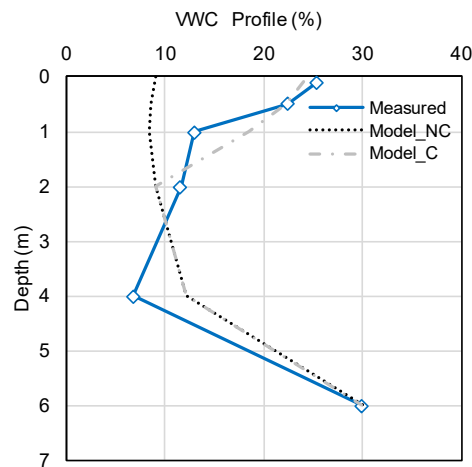
Figure 11. Initial VWC profiles: measured to date 03 June 2019 (continuous blue line), modelled Non-Calibrated (NC) and Modelled Calibrated (C).

For each series, a total of three simulations were carried out, respectively considering different boundary conditions: 1. only precipitation (R), 2. both precipitation and evaporation (Cl), and 3. precipitation and evapotranspiration due to vegetation (VE). For the cases with climate boundary conditions (Cl and VE), a set of meteorological variables (i.e. air temperature, relative humidity, wind speed and solar radiation) were needed to feed the Penman-Monteith equation to determine the evaporation flux. Furthermore, additional information related to the vegetation was also needed for the determination of the evapotranspiration flux. An overview of the effects of vegetation on the hydraulic modelling and the Penman-Monteith equation using SEEP/W was provided in a recent study (Capobianco et al., 2021). Reference values for the vegetation features were used, since no specific investigations have been carried out on the slope. Specifically, the Leaf Area Index (LAI), defined as the projected area of leaves over a unit of land, was set equal to 1.5 for the summer (June-September) and equal to 0 for the autumn and winter period (October-December). The Plant Moisture limit (PML) was set equal to suggested default value from SEEP/W manual (Geoslope, 2012). An arbitrary value of 1 m is selected for the root depth (RD), and the normalized root density (NRD) was considered to have a negative linear trend. Finally, the soil cover fraction (SCF), representing the percentage of soil covered by the canopy, was a proportional function of the LAI (for LAI=0, SCF=0; for LAI=1.5, SCF=1), and the vegetation height, equal to 3 meters, is an average between bushes and tree heights present along the slope. Vegetation could change the soil water retention capability of the root-permeated soil (Scholl et al., 2014; Ng et al., 2016; Leung et al., 2018; Capobianco et al., 2020), however there still is an open debate on whether vegetation reduces or increases

the soil water permeability. Similarly, frost action and drying can be important for infiltration in shallow layers due to shrinkage/cracking and soil heave. Since this aspect goes beyond the scope of this work, the same hydraulic properties of the unsaturated layers were adopted in all simulated cases (Table 3), including those with vegetation. The variables needed for each simulation are listed in Table 4.

Table 4. Simulations in SEEP/W and list of climate and vegetation variables needed for each simulation. PML= Plant Moisture Limit; RD= Root Depth; NRD= Normalized Root Density; SCF= Soil Cover Fraction. Simulations: NC_R = Non-calibrated considering precipitation, NC_Cl = Non-calibrated considering precipitation and evaporation, NC_Cl_VE = Non-calibrated considering precipitation, evaporation and vegetation; C_R = Calibrated considering precipitation, C_Cl = Calibrated considering precipitation and evaporation, C_Cl_VE = Calibrated considering precipitation, evaporation and vegetation.

Series	ID simulation	Climate boundary conditions						Vegetation properties					
		Rainfall/ snowmelt	Temperature	Relative Humidity	Wind speed	Solar radiation	Albedo	LAI	PML	RD	NRD	SCF	Vegetation height
IC Non-calibrated	NC_R	●											
	NC_Cl	●	●	●	●	●	●						
	NC_Cl_VE	●	●	●	●	●	●	●	●	●	●	●	●
IC Calibrated	C_R	●											
	C_Cl	●	●	●	●	●	●						
	C_Cl_VE	●	●	●	●	●	●	●	●	●	●	●	●

6   Results and discussions

6.1   Validation of the hydrogeological model through the measured VWC

The predicted VWC calculated with the SEEP/W module were compared to the measured values. The comparisons were carried out for a 6-months period (i.e., June 2019 - August 2019), considering all the measured depth points and comparing predicted with measured data (i.e., in-situ measurements). Figure 12 compares values and trends of all the VWC simulations (see section 4.3) with time (day), with the in-situ measured VWC for the 6 depths. For the shallowest layers (up to 1 m depth) the model could simulate quite accurately the short-term response to the atmospheric drivers, while at 6 m depth the model was able to reproduce the flat trend of the VWC, with a little underestimation of the observed values of about 5%. On the contrary, at middle depths, between 2 and 4 m, an increase of the VWC with time for all the simulated combinations was observed, in discordance with the measured data, which maintain almost a constant trend. One explanation could be a limitation of the 2-D model, which cannot simulate potential directional flows in 3D that might have occurred locally.
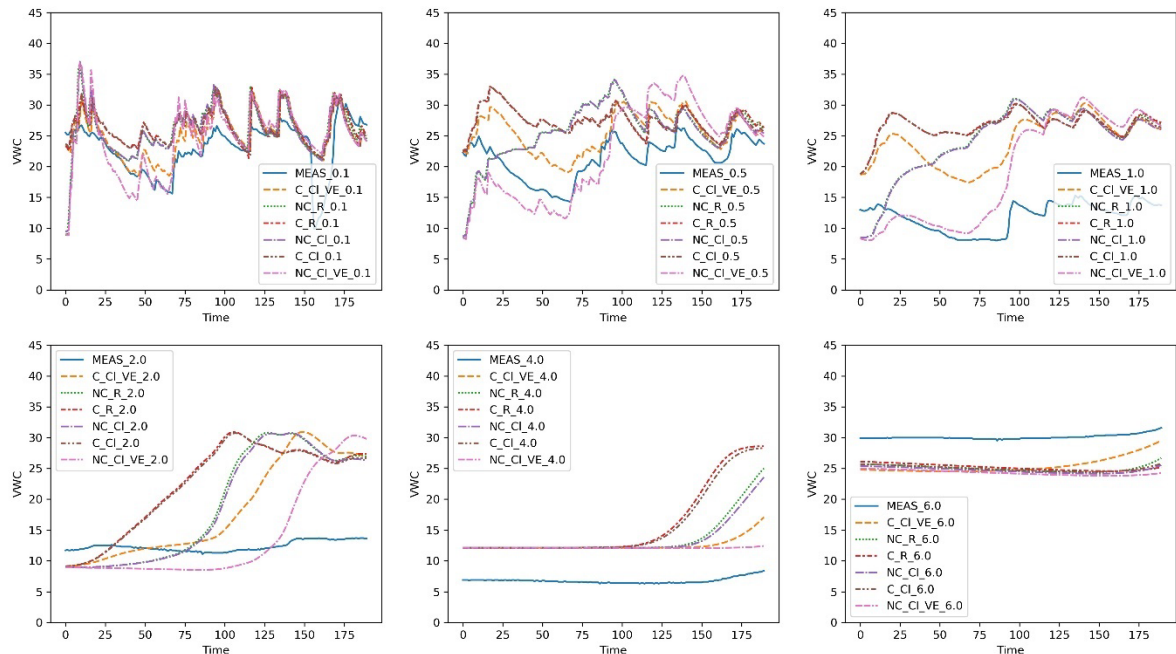

Figure 12. Variation with time of the measured VWC (continuous blue line) and modelled VWC values from the different simulated cases (ref. to Table 4) during the 6-months period of observation respectively at a) 0.1 m depth; b) 0.5 m depth; c) 1 m depth; d) 2 m depth; e) 4 m depth and f) 6 m depth.

Another condition that might have caused this discrepancy between predicted and observed values is the possible presence of an intermediate drainage layer located between 2 and 4 m depth. This would explain the very low VWC recorded in-situ.

A common and simple approach to correlate modelled and observed data is to regress predicted and observed values and compare slope and intercept parameters against the 1:1 bisector line that represents the perfect correlation between the two variables. The disposition of the variables is important because, although the correlation value is the same, the intercept and the slope of each regression differ and, in turn, may change the result of the model evaluation (Pineiro et al., 2008). Pairs of observed-predicted VWC values were respectively plotted in the y-axis and x-axis for each of the 6 sensor depths in Figure 13. The

figure shows the pairs of observed-predicted VWC for the 6 simulated cases for each daily measurement, on the left side the non-calibrated series, and on the right side, the calibrated ones (see Table 3). For almost all the depths, the non-calibrated data series (Figure 13a,b,c) were more scattered, whereas for calibrated simulations (Figure 13d,e,f) the values were less spread and closer to the 1:1 line for almost all the depths. At 2 m and 4 m depth, the discrepancy between measured and modelled data was visible as the points are spread horizontally and not along the bisector line.

Despite the limitations mentioned above, the simulations were, from a slope stability analysis point of view, conservative at almost all depths (apart from 6 m depth), since the predicted VWC points were mostly all located either on the 1:1 line or below it (Figure 13). Few points were located above the 1.1 line. This means that the predicted VWC values were generally higher than the observed values, which in turn would result in predicted soil shear strength on the safe side. This discrepancy can also be justified by the SWRCs used to perform the analyses, since the curves are calculated for the drying phase based on drying tests. For soils with hysteretic behaviour, for the same values of suction, the corresponding VWC in the drying path is higher than the one in the wetting path (Childs and Collis George, 1950; Croney and Coleman, 1954; Millington and Quirk, 1959; Kunze et al. 1968; Mualem, 1974; Hillel, 1982; Hogarth et al. 1988; Pham et al. 2003; Maqsoud et al. 2006; Nuth and Laloui, 2008; Malaya and Sreedeep 2012, Sorbino and Nicotera, 2013; Rianna et al. 2019; Capparelli and Spolverino, 2020; Comegna et al. 2021). Thus, sometimes ignoring the hydraulic hysteresis could mislead the estimation of failure potential (Chen et al 2017) for a slope exposed to a precipitation path (Comegna et al. 2016). It is also worth mentioning that the SWRCs were obtained in the laboratory, while experimental curves in-situ can give different results even though are more difficult to perform. In fact, the impact of soil structure on water retention curves and hydraulic conductivity in the field, relative to small core samples, has been recognized in previous studies (Mirus et al. 2015; Fatichi et al. 2020). In addition, the variability of hydraulic parameters for a field-based SWRC is also smaller compared to a laboratory-based or texture-based SWRC, reflecting also in a smaller variability of the modelled safety factor when using this curve (Thomas et al. 2018). Finally, another limitation of the modelling program is that it can only simulate homogeneous layers, while it has been observed in Heyerdahl et al. (2018) that soil layers 1 (0-6 m) and 2 (6-9 m) are not completely homogeneous, as the proportions of silt, sand and clay is not constant with depth.
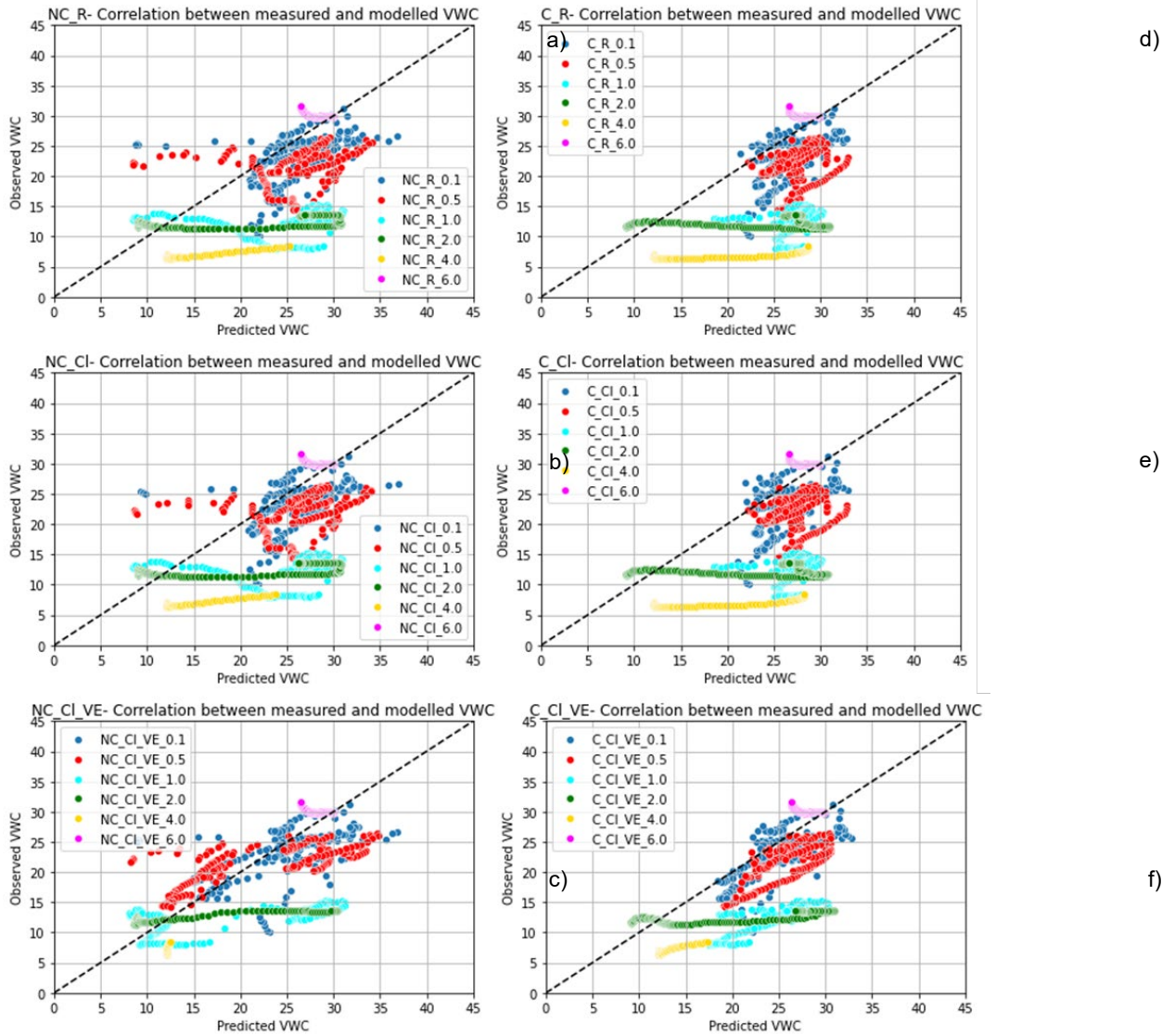
Figure 13. Regression between observed (y-axis) and predicted (x-axis) VWC values and comparison against the 1:1 line (perfect correspondence) for the following simulated cases a) NC_R, b) NC_CL, c) NC_Cl-VE, d) C_R, C_Cl, and f) C_Cl_VE.

6.2 Validation with Taylor diagrams

A detailed graphical comparison of how closely the simulations match the observations, was provided by Taylor diagrams (Taylor, 2001). The similarity between two patterns was quantified in terms of their correlation, their centered root-mean-square difference and their standard deviations (Taylor, 2001). R coefficient, (eq. 2), SDV (eq. 3) RMSD (eq. 4) and bias (eq. 5) were calculated for each couple of predicted-observed datasets (see Section 4.2). The results were plotted in the Taylor diagrams (Figure 14).
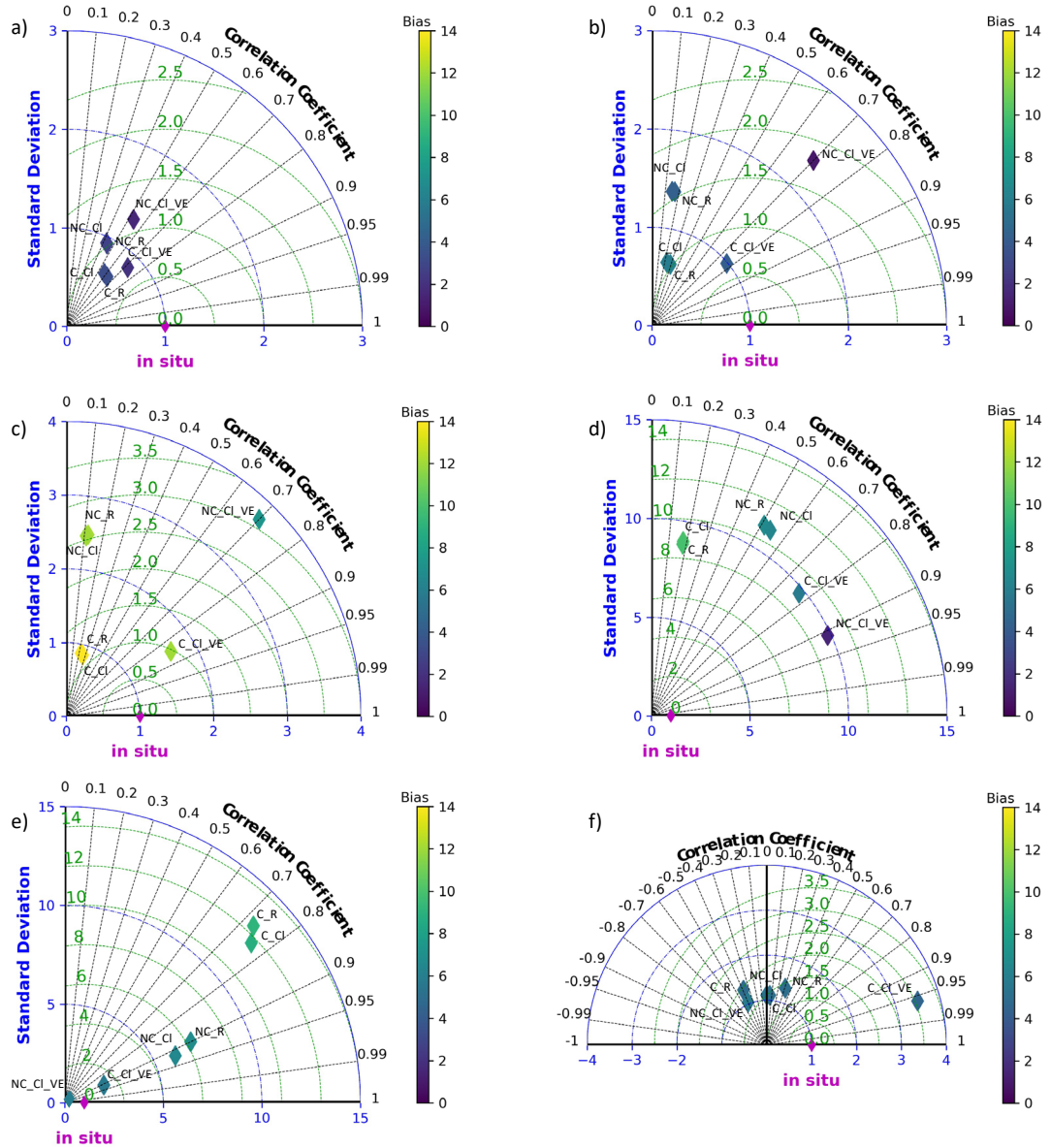
Figure 14. Taylor diagrams comparing modelled and measured VWC respectively for the following depth: a) 0.1 m, b) 0.5 m, c) 1 m, d) 2 m, e) 4 m and f) 6 m. The purple diamond in correspondence to the point 1 of SDV and R, and 0 of RMSD, represents the in-situ condition.

Each diagram plots the comparison between modelled and observed VWC values at different soil depths (0.1, 0.5, 1, 2, 4, 6 meters). Every diamond is representative of a simulation case from Table 3 and is plotted in the diagram as a function of the calculated 'R' coefficient (black curves), SDV (blue curves) and RMSD (green curves); the diamond colour is representative of the bias. The position of each diamond on the plot quantifies how closely that model's simulated SWC pattern matches observations. Ideally, a good model would have relatively high correlation, low RMS errors (Taylor, 2001) and SDV around 1. Furthermore, the darker is the diamond symbol colour the lower is the error in predicting the VWC values. Series-wise, it is possible to confirm that the best simulations are those that belong to the series C, where an initial hydrological adjustment (i.e., calibration) of the VWC was performed. At almost all depths, the values simulated in the C series were closer to the observed in-situ value trends.

Figure 14 shows that the simulation C_Cl_VE generally agrees better with the observations at almost all depths, apart for 2 m and 6 m. The simulation C_Cl_VE shows a very good agreement with the observed VWC at 0.1 and 0.5 meters, highlighting that despite the bigger variability of data observed at the shallowest layers, mostly due to the short-response to atmospheric drivers, the simulation C_Cl_VE agrees with the in-situ trend and values compared to the other simulations. On the contrary, the simulation C_Cl_VE was less able to model the VWC at 2 m. This is immediately visible because RMSD and SDV values were higher than those calculated for other depths, indicating less agreement between the predicted and measured trends. Even though at 2 m (Figure 14d) there is a fairly high correlation (0,77), SDV and RMSD were high (respectively 9,7 and 9,5), and the bias was of about 6%. However, it is important to underline that none of the simulations can correctly model the VWC at 2 m (Figure 14d). At 4 m depth (Figure 14e), the C_Cl_VE simulation showed a good agreement with the observed data, with a bias around 6%. At 6 m (Figure 14f), high correlation (0,97) and low bias, but high SDV (3,5) indicate that the model was able to reasonably predict the trend and the values, but with some pattern variation of the predicted values compared to the measured one. This result can be seen also by looking at Figure 6f, where the simulated VWC has about 5% bias and a slightly different trend compared to the measured one. In summary, these results show that for modelling in-situ VWC it is important to carry out an initial calibration and to perform the analyses considering both vegetation and climatic variables. Furthermore, the validation process is important to prove that the SEEP/W modelling, specifically simulation C_CL_VE, is able to back analyse the hydrogeological conditions within the slope at almost all depths.

6.3 Effectiveness of the hydrogeological model with time

Climate and vegetation change can influence significantly the hydrological behaviour of unsaturated slopes. For example, temperature can change the VWC of the shallowest layers from one season to another, while roots can improve the permeability of the rhizosphere, thus promoting lateral diversion of rainwater and acting like a natural lateral drainage (Balzano et al. 2019). The previous section shows that the simulation C_Cl_VE, considering a preliminary calibration, climate drivers and vegetation, has the highest performance to represent the monitored in-situ conditions. To assess the effectiveness of the hydrogeological model of catching the processes happening throughout the year within the unsaturated layer, the authors carried out an analysis considering different time spans. The Taylor diagrams were used to compare the hydrological modelling for the best-fits of C_Cl_VE, with the measured data (i.e., 0.1, 0.5, 1, 4 meters depth), for three different time spans. A 3-month period, June 2019 - August 2019, and a 12-month period, June 2019 - June 2020, were compared to the 6-month case analysed and showed in Section 5.2.

Figure 15 shows the results of the Taylor diagrams for the modelled VWC variables (simulation C_Cl_VE), at different depths and, respectively, for the periods: 3-month (3M), 6-month (6M) and 12-month (12M). The simulations 3M and 6M had a better match with the measured VWC trends and values compared to the ones of 12M. At 1 m, instead, the 3M simulation had a lower R (0.7) compared to 6M (0.85), but a SDV closer to 1 and the lowest bias value compared to both 6M and 12M. The results suggest that a re-calibration of the numerical modelling should be performed at maximum every 6 months for the studied slope. This indicates that for a time span, up to 6 months, the model was able to accurately simulate the measured data.
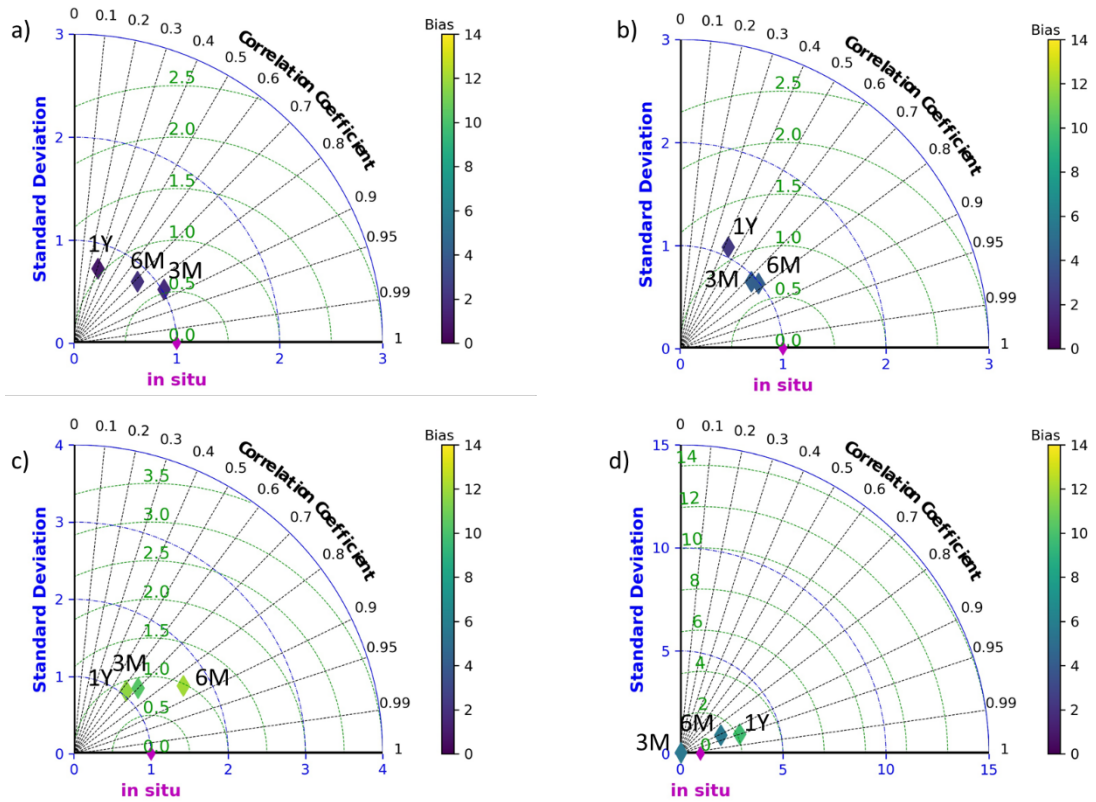
Figure 15. Taylor diagrams comparing modelled and measured VWC of the combination C_Cl_VE for 3 months (3M), 6 months (6M) and 12 months (12M) period, respectively for the following depths: a) 0.1 m, b) 0.5 m, c) 1 m, d) 4 m. The purple diamond in correspondence to the point 1 of SDV and R, and 0 of RMSD, represents the in-situ condition.

6.4   Stability analysis

Figure 16 shows the calculated Factor of Safety (FS) vs time, for representative simulations of both non-calibrated (i.e., NC_R) and calibrated series (i.e., C_Cl_VE and C_Cl) for the 6-month period. Overall, small drops of FS can be seen after a single precipitation event, while the main trend increased in summer and decreased in autumn.

Firstly, a comparison between the calibrated simulations (C_Cl and C_Cl_VE in Figure 16) was carried out, to quantify the effect of vegetation on slope stability. The simulation considering climate variables without vegetation (C_Cl) overlaps with the vegetated one (C_Cl_VE) in the first part of the simulated period, and it tends to get closer to it again in last part. This is because the parameters LAI and SCF were considered in the model only in the summer period, to simulate the flourishing period of vegetation. A variation of around 5% was found between the two calibrated cases (C_Cl and C_Cl_VE). This difference was indeed given by input of vegetation parameters in the slope stability analysis. The FS stays almost constant through August for both combinations, after which it starts to decrease in the middle of the wet season (i.e., November/December), until it goes below 1 for the case C_Cl. This might be due to the combined effect of more frequent rainfall events, and the reduced evaporation due to the decreased temperature. For the case C_Cl_VE, the trend is the same with the exception that it never goes below 1. A final comparison was carried out between the best (C_Cl_VE) and the worst (NC_R) fit simulations; the latter had no initial

calibration, and no climate conditions other than rainfall. As a result, the FS calculated for NC_R was always below the limit value 1, and around 0.85-0-95. This situation is not realistic since no evidence of failure has been observed in-situ.

A maximum of 18% difference was found between the two simulations, highlighting the importance of climate boundary conditions and vegetation in the correct evaluation of unsaturated slope stability (Capobianco et al., 2021). The lowest FS values were computed in correspondence to the date 22/11/2019 and, were, respectively FS= 1.023 (C_Cl_VE), 0.99 (C_Cl) and 0.86 (NC_R). This was after the rainfall period of about one month, confirming that the autumn season is where most likely failures can occur. Figure 17 shows the critical sliding surface in the period of analysis calculated for the case N_R. The region where potential sliding surfaces with FS<1 are located, is also indicated in red. The results are in accordance with literature, indicating that the primary influential factor for landslides initiation is a combination of initial water content, rainfall duration and intensity and antecedent rainfall (Pagano et al. 2010; Li et al. 2020), and that also the hydrological reinforcement of vegetation is reduced during the wet season (Chirico et al. 2013). It is well recognized that roots can reinforce the soil-root composite material also through additional cohesion (Wu et al. 1979; Nilaweera and Nutalaya 1999; Cazzuffi et al. 2006; Wu 2013; Leung et al. 2015, Dias et al. 2017 Masi et al., 2021), basal and lateral root reinforcement (Schwarz et al. 2010), increased friction angle (Foresta et al., 2019) and overall increased tensile strength (Fraccica et al., 2020); however in this specific study, no additional mechanical reinforcement due to vegetation was added the properties of the shallowest soil layers, resulting in a more conservative slope stability analysis.
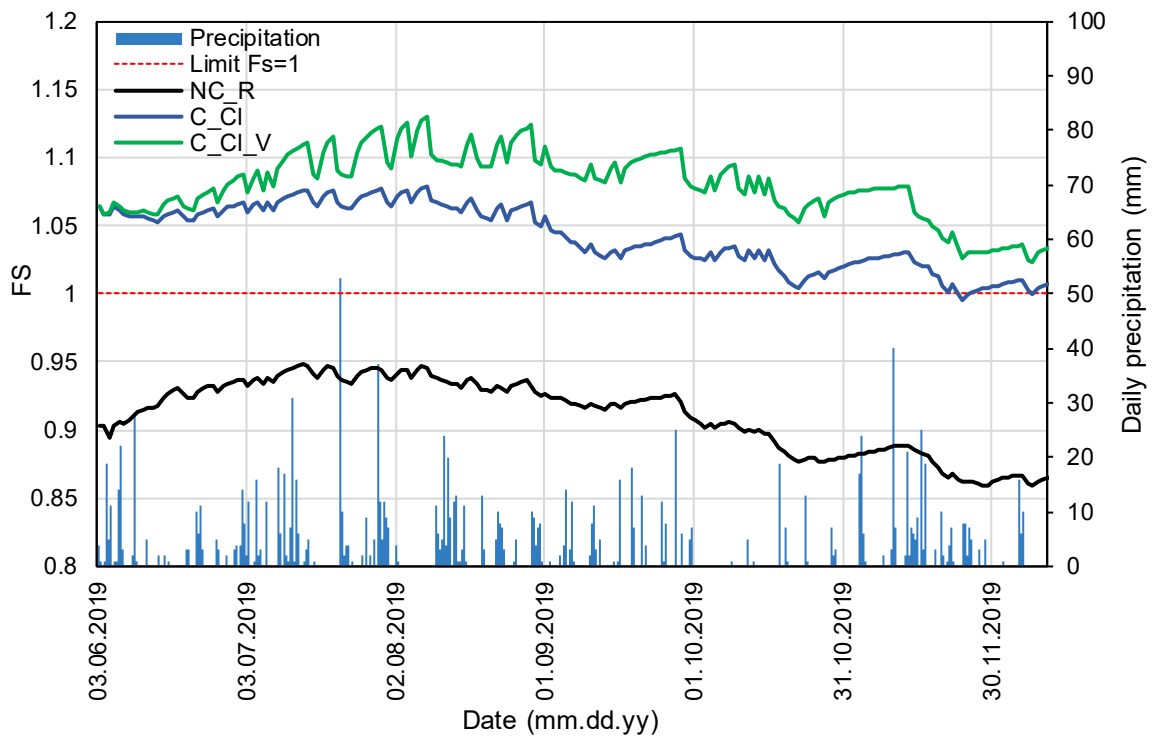
Figure 16. FS vs time for relevant simulated cases for a 6-month period: best fit case with (C_Cl_VE) and without vegetation (C_Cl) and worst simulated case (N_R). The lowest FS values were computed in correspondence o the date 22/11/2019 and were respectively FS= 1.023 (C_Cl_VE), 0.99 (C_Cl) and 0.86 (N_R).
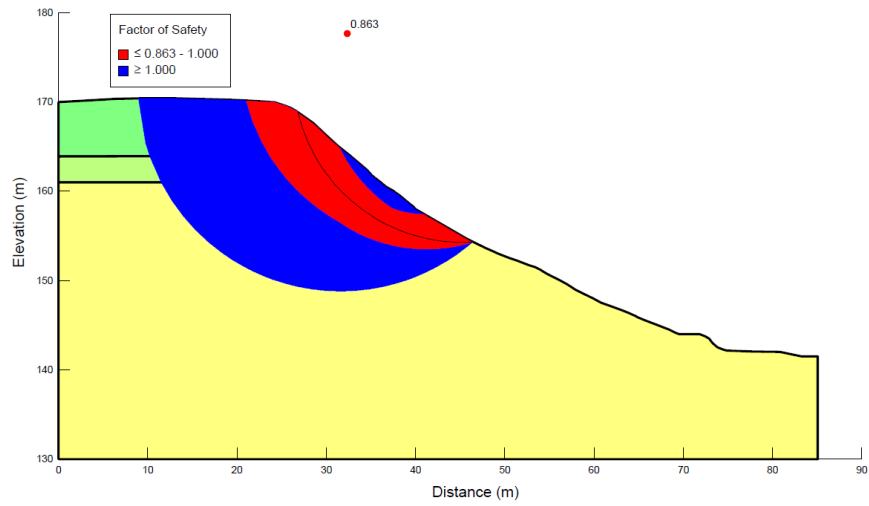
Figure 17. Sliding surfaces computed for the case N_R. In red the position of the sliding surfaces with a potential FS <1.

7   Concluding remarks

This work presented the monitoring and modelling phases for an unsaturated slope in Norway, with a special emphasis on the role of calibration, validation and effectiveness in time of the hydrological model used to assess the behaviour of the unsaturated zone. Two series of simulations were carried out for a 6-month period, one considering an initial calibration of the VWC profile (C), and another one where no initial calibration has been conducted (NC). For each series a total of three simulations were performed, respectively including: precipitation; precipitation and climate parameters; precipitation, climate parameters and effects of vegetation. The paper described the validation of the different simulations with observed in situ measurements of VWC. The comparison carried out using Taylor diagrams showed the importance of including a VWC preliminary calibration as well as precipitation (rainfall and snowmelt), climatic parameters and vegetation in the back analysis. A good agreement between the predicted and the observed hydrogeological variables at different depths was observed, despite all the limitations of the 2-D numerical model SEEP/W. The simulation C_Cl_VE was able to adequately reproduce the observed in-situ VWC conditions at different depths for the selected 6-month period of the analysis. The effectiveness of the hydrological model, for the best simulation, in back-calculating VWC, was tested for 3 different time spans: 3-month, 6-month, 1 year. The results showed that, the accuracy and performance of the SEEP/W model decreased with time in simulating the in-situ hydrogeological conditions. This finding outlines the need of a periodic recalibration (at maximum every 6 months) of the VWC profile and a continuous validation of the SEEP/W model. Although the authors found that up to 6 months can be a fair frequency period to recalibrate the model for the studied slope, this might change from year to year and might not be the case for a different slope in a different environment.

The stability analyses carried out for the 6-month period highlighted that the hydrological variability becomes a crucial aspect when modelling the stability of an unsaturated slope. The comparison between the FS of the most relevant simulated cases showed that up to 18% of variability can be obtained in the slope stability calculation, depending on the complexity of the boundary conditions used in the model. The performed analyses showed that a less complex approach resulted in a considerably lower FS. In addition, the presence of vegetation plays an important role, especially in the late spring/summer periods, increasing the FS through its hydrological reinforcement, by reducing VWC and increasing suction (comparison of C_Cl_VE with C_Cl).

Further work will couple VWC measurements with recently installed tensiometers in the unsaturated layer. The pairs of suction-VWC sensor readings will, then, be used to adjust the SWRCs. This will provide more detailed information on the in-situ wetting-drying cycles of the slope response due to atmospheric drivers, leading to an improved analysis of the hydrogeological conditions and, thus, an even more precise stability analysis. In conclusion, the procedures described in this paper can be seen as a preliminary step towards a remote real-time slope stability analysis at a slope scale. Additional simulations need to be carried out changing the rainfall input, in order to collect enough data that can serve as input for training machine learning algorithms to detect combinations of variables that lead to FS<1. Finally, the possibility to have all the monitored data collected by means of a datalogger into a cloud system, which can feed directly the machine learning algorithms, is the idea behind the definition of a real-time warning system at a slope scale. The final aim of this pilot study in Eidsvoll, Norway is, indeed, to establish a real-time local warning system through the internet of things (IoT), leading to the possibility of remotely predict the stability of the slope based on in-situ data, forecasted rainfall and snowmelt data.

References

Albergel C, Rosnay P D, Gruhier C, Muñoz-Sabater J, Hasenauer S, Isaksen L, Kerr Y, Wagner W (2012) Evaluation of remotely sensed and modelled soil moisture products using global ground-based in situ observations. Remote Sens. Environ. 118: 215–226. https://doi.org/10.1016/j.rse.2011.11.017

Allen R G, Pereira L S, Raes D, Smith M (1998) Crop evapotranspiration - Guidelines for computing crop water requirements - FAO Irrigation and drainage paper 56. Food and Agriculture Organization of the United Nations. ISBN 92-5-104219-5

Alonso E, Gens A, Lloret A, Delahaye C (1995) Effect of rain infiltration on the stability of slopes. In Proceedings of the first International Conference on unsaturated Soils.

Anderson S A, Sitar N (1995) Analysis of rainfall-induced debris flows. Journal of Geotechnical Engineering 121: 544-552. https://doi.org/10.1061/(ASCE)0733-9410(1995)121:7(544)

Balzano B, Tarantino A, Ridley A (2019) Preliminary analysis on the impacts of the rhizosphere on occurrence of rainfall-induced shallow landslides. Landslides, 16(10), 1885-1901. https://doi.org/10.1007/s10346-019-01197-5

Capobianco V, Cascini L, Cuomo S, Foresta V (2020) Wetting-Drying Response of an Unsaturated Pyroclastic Soil Vegetated with Long-Root Grass. Environmental Geotechnics, 40:1-18. https://doi.org/10.1680/jenge.19.00207

Capobianco V, Robinson K, Kalsnes B, Ekeheien C, Høydal Ø (2021) Hydro-Mechanical Effects of Several Riparian Vegetation Combinations on the Streambank Stability—A Benchmark Case in Southeastern Norway. Sustainability, 13(7), 4046. https://doi.org/10.3390/su13074046

Capparelli G, Spolverino G (2020) An Empirical Approach for Modeling Hysteresis Behavior of Pyroclastic Soils. Hydrology, 7(1), 14. https://doi.org/10.3390/hydrology7010014

Casagli N, Dapporto S, Ibsen M Č, Tofani V, Vannocci P (2006) Analysis of the landslide triggering mechanism during the storm of 20th–21st November 2000, in Northern Tuscany. Landslides 3:13-21. https://doi.org/10.1007/s10346-005-0007-y

Cascini L, Cuomo S, Pastor M, Sorbino G (2010) Modeling of Rainfall-Induced Shallow Landslides of the Flow-Type. J Geotech Geoenviron Eng 136:85-98. https://doi.org/10.1061/(ASCE)GT.1943-5606.0000182

Cazzuffi D, Corneo A, Crippa E (2006) Slope stabilisation by perennial "gramineae" in southern Italy: plant growth and temporal performance. Geotech Geol Eng. 24: 429–447. doi:10.1007/s10706-005-4144-9

Chen P, Mirus B, Ning L, Godt JW (2017) Effect of Hydraulic Hysteresis on Stability of Infinite Slopes under Steady Infiltration, J Geotech Geoenviron Eng. 143(9) https://doi.org/10.1061/(ASCE)GT.1943-5606.0001724

Childs EC, Collis-George N (1950) The permeability of porous materials. Proc R Soc 201A:392–405. https://doi.org/10.1098/rspa.1950.0068

Chirico G B, Borga M, Tarolli P, Rigon R, Preti F (2013) Role of vegetation on slope stability under transient unsaturated conditions. Procedia Environmental Sciences, 19, 932-941. https://doi.org/10.1016/j.proenv.2013.06.103

Comegna L, Damiano E, Greco R et al. (2016) Field hydrological monitoring of a sloping shallow pyroclastic deposit. Can Geotech J 53: 1125–1137. https://doi.org/10.1139/cgj-2015-0344

Comegna L, Damiano E, Greco R, Guida A, Olivares L, Picarelli L (2013) Effects of the vegetation on the hydrological behavior of a loose pyroclastic deposit. Procedia Environmental Sciences, 19:922-931. https://doi.org/10.1016/j.proenv.2013.06.102

Comegna L, Damiano E, Greco R, Olivares L, Picarelli L (2021) The hysteretic response of a shallow pyroclastic deposit (2021). Earth Syst. Sci. Data, 13:2541-2553, https://doi.org/10.5194/essd-13-2541-2021

Comegna L, Rianna G, Lee S, Picarelli L (2016) Influence of the wetting path on the mechanical response of shallow unsaturated sloping covers, Computers and Geotechnics 73:164-169, https://doi.org/10.1016/j.compgeo.2015.11.026

Croney D, Coleman JD (1954) Soil structure in relation to soil suction. J Soil Sci 5:75–84. https://doi.org/10.1111/j.1365-2389.1954.tb02177.x

Dias, A. S., Pirone, M., & Urciuoli, G. (2017, May). Review on the methods for evaluation of root reinforcement in shallow landslides. In Workshop on World Landslide Forum (pp. 641-648). Springer, Cham.

Duong T T, Do D M, Yasuhara K (2019) Assessing the Effects of Rainfall Intensity and Hydraulic Conductivity on Riverbank Stability. Water, 11:741. https://doi.org/10.3390/w11040741

Foresta V, Capobianco V, Cascini L (2020) Influence of grass roots on shear strength of pyroclastic soils. Can Geotech J, 57:1320-1334. https://doi.org/10.1139/cgj-2019-0142

Fraccica A, Romero E, Fourcaud T, Sondon M, Gandarillas L (2020) Tensile strength of a vegetated and partially saturated soil. In E3S Web of Conferences (Vol. 195, p. 03001). DOI : 10.1051/e3sconf/202019503001

Fredlund D G, Rahardjo H (1993) Soil mechanics for unsaturated soils. John Wiley & Sons.

Fredlund D G, Morgenstern N R, Widger R A (1978) The shear strength of unsaturated soils. Can Geotech J, 15(3), 313-321. https://doi.org/10.1139/t78-029

Gariano S L, & Guzzetti F (2016) Landslides in a changing climate. Earth-Science Reviews, 162, 227-252. https://doi.org/10.1016/j.earscirev.2016.08.011

GEO-SLOPE International Ltd. Seepage Modeling with SEEP/W (2012) Available online: http://downloads.geo-slope.com/geostudioresources/8/0/6/books/seep%20modeling.pdf?v=8.0.7.6129 (accessed on 29 March 2020).

Godt JW, McKenna JP (2008) Numerical modeling of rainfall thresholds for shallow landsliding in the Seattle, Washington area. In: Baum RL et al. (eds) Landslides and engineering geology of the Seattle, Washington area, Reviews in Engineering Geology, vol 20. Geological Society of America, Boulder, pp 121–135. https://doi.org/10.1130/2008.4020(07)

Greco R, Comegna L, Damiano E, Guida A (2017) Investigation on the hydraulic parameters affecting shallow landslide triggering in a pyroclastic slope. In: Mikoš M et al. (eds) Fourth world landslide forum, Advancing culture of living with landslides, vol 2. pp 659–667. https://doi.org/10.1007/978-3-319-53498-5

Hanssen-Bauer I, Førland EJ, Hisdal H, Mayer S (2017) Climate in Norway 2100 – a knowledge base for climate adaptation. NCCS Report no. 1/2017 (www.klimaservicesenter.no)

Heyerdahl H, Hoydal O A, Kvistedal Y, Gisnas K G, Carotenuto P (2018) Slope instrumentation and unsaturated stability evaluation for steep natural slope close to railway line. In UNSAT 2018: The 7th International Conference on Unsaturated Soils.

Hogarth W, Hopmans J, Parlange JY (1988) Application of a simple soil water hysteresis model. J Hydrol 98:21–29. https://doi.org/10.1016/0022-1694(88)90203-X

Krzeminska D, Kerkhof T, Skaalsveen K, Stolte J (2019) Effect of riparian vegetation on stream bank stability in small agricultural catchments. Catena, 172:87-96. https://doi.org/10.1016/j.catena.2018.08.014

Kunze RJ, Uehara G, Graham K (1968) Factors important in the calculation of hydraulic conductivity. Soil Sci Soc Am J 32:760–765. https://doi.org/10.2136/sssaj1968.03615995003200060020x

Leung AK, Boldrin D, Liang T et al. (2018) Plant age effects on soil infiltration rate during early plant establishment. Géotechnique 68(7): 646–652, https://doi.org/10.1680/jgeot.17.T.037

Leung F T, Yan W M, Hau B C, Tham, L G (2015) Root systems of native shrubs and trees in Hong Kong and their effects on enhancing slope stability. Catena, 125: 102–110. doi:10.1016/j.catena.2014.10.018

Li L, Ju N, He C, Li C, Sheng D (2020) A computationally efficient system for assessing near-real-time instability of regional unsaturated soil slopes under rainfall. Landslides, 17:4, 893-911. https://doi.org/10.1007/s10346-019-01307-3

Li A G, Tham L G, Yue Z Q, Lee C F, Law K T (2005a) Comparison of field and laboratory soil–water characteristic curves. J Geotech Geoenviron Eng. 131:1176-1180. https://doi.org/10.1061/(ASCE)1090-0241(2005)131:9(1176)

Li A G, Yue Z Q, Tham L G, Lee C F, Law K T (2005b) Field-monitored variations of soil moisture and matric suction in a saprolite slope. Can Geotech J. 42:13-26. https://doi.org/10.1139/t04-069

Liu Y, Yang Y, Yue X (2018) Evaluation of satellite-based soil moisture products over four different continental in-situ measurements. Remote Sensing, 10: 1161. https://doi.org/10.3390/rs10071161

Lu N, Godt J W, Wu D T (2010) A closed-form equation for effective stress in unsaturated soil. Water Resour Res, 46(5). https://doi.org/10.1029/2009WR008646

Masi EB, Segoni S, Tofani V (2021) Root Reinforcement in Slope Stability Models: A Review. Geosciences 2021, 11, 212. https://doi.org/10.3390/geosciences11050212

Malaya C, Sreedeep S (2012) Critical review on the parameters influencing soil-water characteristic curve. Journal of Irrigation and Drainage Engineering, 138:55-62. https://doi.org/10.1061/(ASCE)IR.1943-4774.0000371

Maqsoud AB, Aubertin B, Mbonimpa M (2006) Modification of the predictive MK model to integrate hysteresis of the water retention curve. In: Miller GA, Zapata CE, Houston SL, Fredlund DG (eds) Carefree, Arizona, 2465–2476. https://doi.org/10.1061/40802(189)210

McGuire LA, Rengers FK, Kean JW, Coe JA, Mirus BB, Baum RL, Godt JW (2016) Elucidating the role of vegetation in the initiation of rainfall-induced shallow landslides: insights from an extreme rainfall event in the Colorado Front Range. Geophys Res Lett 43(17):9084–9092. https://doi.org/10.1002/2016GL070741

Melchiorre C, Frattini P (2012) Modelling probability of rainfall-induced shallow landslides in a changing climate, Otta, Central Norway. Climatic change, 113:413-436. https://doi.org/10.1007/s10584-011-0325-0

Millington RJ, Quirk JP (1959) Permeability of porous media. Nature 183:387–388

Mirus BB (2015) Evaluating the importance of characterizing soil structure and horizons in parameterizing a hydrologic process model. Hydrol Process 29(21):4611–4623. https://doi.org/10.1002/hyp.10592

Morgenstern, NR, Price, VE, (1965) The Analysis of the Stability of General Slip Surfaces. Geotechnique, Vol. 15, pp. 79-93.

Ng CWW, Ni JJ, Leung AK and Wang ZJ (2016) A new and simple water retention model for root-permeated soils. Géotechnique Letters 6:106–111, https://doi.org/10.1680/jgele.15.00187

Ng C, Pang Y (2000) Influence of stress state on soil-water characteristics and slope stability. Journal of geotechnical and geoenvironmental engineering 126:157-166. https://doi.org/10.1061/(ASCE)1090-0241(2000)126:2(157)

Nilaweera N S, Nutalaya P (1999) Role of tree roots in slope stabilisation. Bull Eng Geol Environ, 57: 337–342. doi:10.1007/s100640050056

Nuth M, Laloui L (2008) Advances in modelling hysteretic water retention curve in deformable soils. Comput Geotech 35:835–844. https://doi.org/10.1016/j.compgeo.2008.08.001

Pagano L, Picarelli L, Rianna G, Urciuoli G (2010) A simple numerical procedure for timely prediction of precipitation-induced landslides in unsaturated pyroclastic soils. Landslides, 7(3), 273-289. DOI 10.1007/s10346-010-0216-x

Pagano L, Reder A, Rianna G (2014) Experiments to investigate the hydrological behaviour of volcanic covers. Procedia Earth and Planetary Science, 9:14-22. https://doi.org/10.1016/j.proeps.2014.06.013

Pagano L, Reder A, Rianna G (2019) Effects of vegetation on hydrological response of silty volcanic covers. Can Geotech J, 56:1261-1277. https://doi.org/10.1139/cgj-2017-0625

Peranić J, Jagodnik V, Arbanas Ž (2019) Rainfall infiltration and stability analysis of an unsaturated slope in residual soil from flysch rock mass. Proceedings of the XVII ECSMGE-2019 "Geotechnical Engineering Foundation of the Future", Reykjavik, Iceland, 1-6. doi: 10.32075/17ECSMGE-2019-0906

Piciullo L, Calvello M, Cepeda J M (2018) Territorial early warning systems for rainfall-induced landslides. Earth-Science Reviews, 179, 228-247. https://doi.org/10.1016/j.earscirev.2018.02.013

Pham HQ, Fredlund DG, Barbour SL (2005) A study of hysteresis models for soil–water characteristic curves. Can Geotech J 42:1548–1568. https://doi.org/10.1139/t05-071

Rahardjo H, Lee T, Leong E, Rezaur R (2005) Response of a residual soil slope to rainfall. Can Geotech J 42:340-351. https://doi.org/10.1139/t04-101

Rahimi A, Rahardjo H, Leong E C (2011) Effect of Antecedent Rainfall Patterns on Rainfall-Induced Slope Failure. J Geotech Geoenviron 137:483-491. https://doi.org/10.1061/(ASCE)GT.1943-5606.0000451

Rianna G, Pagano L, Urciuoli G (2014) Rainfall patterns triggering shallow flowslides in pyroclastic soils. Engineering Geology, 174: 22-35. https://doi.org/10.1016/j.enggeo.2014.03.004

Richards L A (1931) Capillary Conduction of Liquids Through Porous Mediums. Physics, Vol. 1. https://doi.org/10.1063/1.1745010

Saloranta T (2012) Simulating snow maps for Norway: Description and statistical evaluation of the seNorge snow model. The Cryosphere Discussions 6(6):1323-1337. DOI: 10.5194/tc-6-1323-2012

Sarma C P, Dey A, & Krishna A M (2015) Landslide Early Warning based on Geotechnical Slope Stability Model for the Guwahati Region. In 50th Indian Geotechnical Conference, Pune, India.

Scholl P, Leitner D, Kammerer G et al. (2014) Root induced changes of effective 1D hydraulic properties in a soil column. Plant and Soil 381(1–2): 193–213, https://doi.org/10.1007/s11104-014-2121-x

Sorbino G, Nicotera M V (2013) Unsaturated soil mechanics in rainfall-induced flow landslides. Eng. Geol. 165:105–135. https://doi.org/10.1016/j.enggeo.2012.10.008

Statens vegvesens handbook, (2018) Håndbok V220 Geoteknikk i vegbygging. https://www.vegvesen.no/siteassets/content/vedlegg/handboker/hb-v220-2018.pdf

Taylor K E (2001) Summarizing multiple aspects of model performance in a single diagram. J Geophys Res, 106:183-7192. https://doi.org/10.1029/2000JD900719

Thomas MA, Mirus BB, Collins BD, Lu N, Godt JW, (2018) Variability in soil-water retention properties and implications for physics-based simulation of landslide early warning criteria. Landslides, https://doi.org/10.1007/s10346-018-0950-z

Vanapalli S K, Fredlund D G, Pufahl D E, Clifton A W (1996) Model for the prediction of shear strength with respect to soil suction. Can Geotech J, 33:379-392. https://doi.org/10.1139/t96-060

Wu T H (2013). Root reinforcement of soil: review of analytical models, test results, and applications to design. Can Geotech J, 50(3):259–274. doi:10.1139/cgj-2012-0160

Wu T H, McKinnell W P III, Swanston D N (1979) Strength of tree roots and landslides on Prince of Wales Island, Alaska. Can Geotech J, 16(1): 19–33. doi:10.1139
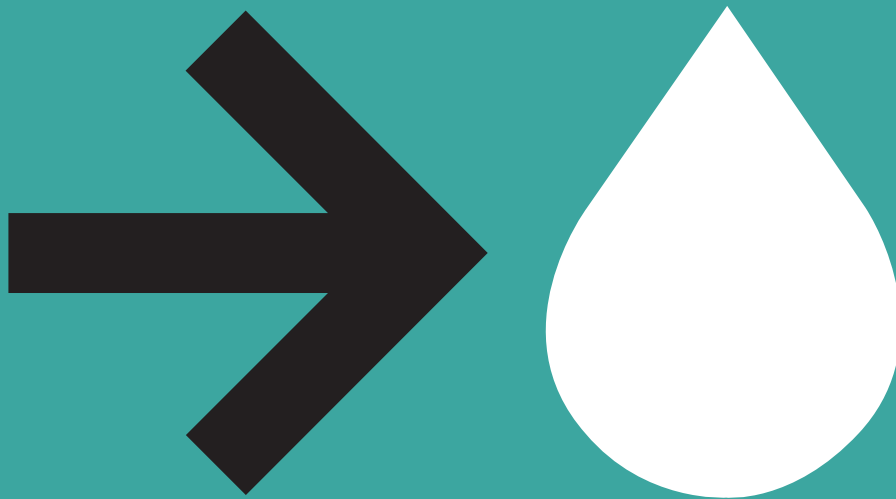
CONSORTIUM

Private sector

SKANSKA

MESTERHUS

Multiconsult

Finans Norge

SKJÆVELAND GRUPPEN

NORGESHUS

Leca

isola

Public sector

Statens vegvesen

Noregs vassdrags- og energidirektorat
NVE

AVINOR

Jernbane-direktoratet

STATSBYGG

TRONDHEIM KOMMUNE

Research & education

SINTEF

BI

NTNU

Meteorologisk institutt

NGI